

Localization Study of a Regularized Variational Damage Model

Milan Jirásek^a, Jan Zeman^a

^a*Department of Mechanics, Faculty of Civil Engineering, Czech Technical University in Prague, Thákurova 7, 166 29 Prague 6, Czech Republic*

Abstract

The paper presents a detailed analysis and extended formulation of a rate-independent regularized damage model proposed by Mielke and Roubíček (2006). Localization properties are studied in the context of a simple one-dimensional problem, but the results reveal the fundamental features of the basic model and of its modified versions. The initial bifurcation from a uniform solution is described analytically while the complete failure process is studied numerically. Modifications of the regularizing term and of the dissipation distance are introduced and their effect on the global response is investigated. It is shown that, with a proper combination of model parameters, a realistic shape of the load-displacement diagram can be achieved and pathological effects such as extremely brittle response or expansion of the damage zone accompanied by stress locking can be eliminated.

Keywords. damage, failure, dissipation, non-locality, variational approach, bifurcation

1. Introduction

In engineering mechanics, *damage* is understood as a load-induced evolution of microstructural defects, resulting in a reduced macroscopic material integrity. Phenomenological constitutive models of damage characterize such irreversible phenomena by an *internal* damage variable (Kachanov, 1958), which is closely related to the reduction of the secant modulus of elasticity. Since the seminal contribution of Bažant (1976), it has been well-understood that such a description within the

Email addresses: Milan.Jirasek@fsv.cvut.cz (Milan Jirásek), zemanj@cml.fsv.cvut.cz (Jan Zeman)

URL: <http://mech.fsv.cvut.cz/~milan> (Milan Jirásek), <http://mech.fsv.cvut.cz/~zemanj> (Jan Zeman)

framework of local (i.e. scale-free) continuum mechanics leads to an ill-posed problem, resulting in localization of damage growth into an arbitrarily small region. As a remedy to this pathology, a plethora of non-local rate-independent continuum theories, based on integral, explicit and implicit gradient approaches, have been proposed to introduce an *internal length scale* into the description, see e.g. [Bažant and Jirásek \(2002\)](#) for a representative overview. Despite a significant increase in objectivity offered by the enhanced continuum theories, the non-local damage formulations often suffer from the fact that the non-local variables are introduced into the model in an ad-hoc fashion, thus violating basic constraints of thermodynamics. In addition, since the principle of local action is no longer valid, such inconsistencies are rather difficult to detect, especially in the multi-dimensional setting, e.g. [Simone et al. \(2004\)](#). Fortunately, as demonstrated by [Jirásek \(1998\)](#) and confirmed by a number of independent studies, e.g. ([Peerlings et al., 2001](#); [Jirásek and Rolshoven, 2003](#); [Di Luzio and Bažant, 2005](#); [Engelen et al., 2006](#); [Jirásek and Rolshoven, 2009a,b](#)), a simple one-dimensional study of the localization behavior can serve as a convenient “filter” test, allowing to pinpoint various inconsistencies in the formulation of a constitutive model. The same point of view has recently been adopted by [Pham et al. \(2011\)](#) and [Pham and Marigo \(2013\)](#), who investigated various aspects of the response a wide class of energy-based gradient damage models under displacement-controlled uniaxial tension. These works build on a variational framework for local and gradient-based models developed by [Pham and Marigo \(2010a,b\)](#), in which evolution follows from physically sound principles of stability, energy balance, and irreversibility, expressed using a single energy functional. In particular, [Pham et al. \(2011\)](#) concentrates on the stability of homogeneous solutions, while in the follow-up work ([Pham and Marigo, 2013](#)) the authors study in detail the behavior inside the damaged zone and its implications for the structural response. In both cases, the material constitutive law is incorporated in the model indirectly by means of parametrized energy families with parameters adjusted to reproduce the local stress-strain response of the material under investigation. The purpose of our paper is to complement these developments with detailed localization studies for gradient damage models based on the commonly used local stress-strain diagrams. To this purpose, we start from the discussion of an elementary elastic-brittle model regularized by the gradient of damage in the spirit of [Frémond and Nedjar \(1996\)](#); see Section 2. Our description builds on a general framework established by Mielke and co-workers, see e.g. [Mielke \(2005\)](#) for an overview, developed to study the evolution of general irreversible rate-independent systems, which has been applied to rigorous analysis of gradient damage models and their numerical approximation ([Mielke and Roubíček, 2006](#); [Bouchitté et al., 2009](#); [Mielke et al., 2010](#); [Thomas and Mielke, 2010](#); [Mielke, 2011a](#)). The variational formulation presented in Section 2 is thus

based on a stored energy functional, quantifying the reversibly stored energy, and a dissipation distance accounting for the irreversible changes. The stored energy is further decomposed into a standard (elastic) part and a regularizing part which introduces a characteristic length into the formulation.

Section 3 presents a study of the localization behavior of the model, utilizing arguments of local incremental energy minimization. Following our recent developments (Jirásek et al., 2013), in Section 3.1 we show that the damage profiles during the damage evolution must be continuously differentiable in space, thereby justifying the assumption made by (Pham and Marigo, 2013, Remark 2), and derive the continuity conditions at the interface between elastic and damaging regions, as well the governing equations to be satisfied in the region experiencing damage. These conditions are employed in Section 3.2 to characterize the elastic response, in Section 3.3 to obtain an analytical solution to the damage profile at the onset of damage, and in Section 3.4 to study the response at later stages by means of a numerical procedure described in Appendix A. It turns out that the model is regularized in the sense that the energy dissipation is finite, but the global response is extremely brittle, especially at late stages of the failure process. This motivates the search for modifications which could lead to load-displacement diagrams that better correspond to the actual behavior of quasibrittle materials.

In Section 4, the elastic-brittle core of the model is replaced by linear or exponential softening via modifications of the dissipation distance. In Section 5, an elastic-brittle model with the regularizing part of the stored energy dependent on the gradient of a modified internal variable is developed and its alternative interpretation in terms of a variable characteristic length is suggested. Finally, Section 6 combines the linear or exponential softening with variable characteristic length.

2. Variational formulation of elastic-brittle model

We consider a prismatic bar of initial length L , subjected to displacement-controlled uniaxial tensile loading. In the sequel, the bar will be represented by the interval $\Omega = (-L/2; L/2)$, with boundary $\Gamma = \{-L/2, L/2\}$ (consisting of two points) subjected to the Dirichlet loading $u_D(t) : \Gamma \rightarrow \mathbb{R}$, where $t \in [0; T]$ denotes the (pseudo-) time; see Figure 1. For the sake of simplicity, we denote by e the bar elongation (change of length), i.e., we set $e(t) = u_D(t, L/2) - u_D(t, -L/2)$ in what follows.

Following the standard thermodynamic approach to constitutive modeling, summarized e.g. in Chapter 25 of Jirásek and Bažant (2002), a state of the system is described using *admissible* displacement and damage fields $\hat{u} : \Omega \rightarrow \mathbb{R}$ and $\hat{\omega} : \Omega \rightarrow \mathbb{R}$. Formally, we write

$$\hat{u} \in \mathbb{K}(t) = \{ \hat{u} \in W^{1,2}(\Omega), \hat{u}(x)|_{\Gamma} = u_D(t) \} \quad (1)$$

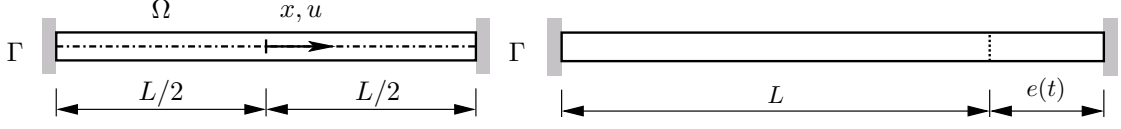


Figure 1: Bar under uniaxial displacement-controlled tension.

$$\widehat{\omega} \in \mathbb{Z} = \{ \widehat{\omega} \in W^{1,2}(\Omega), 0 \leq \widehat{\omega}(x) \leq 1 \text{ in } \Omega \} \quad (2)$$

where $\mathbb{K}(t)$ denotes the set of kinematically admissible displacements at time t , \mathbb{Z} stands for the set of admissible damage fields, and $W^{1,2}(\Omega)$ is the Sobolev space of functions with square-integrable distributional derivatives; see e.g. [Rektorys \(1982\)](#).

Within the adopted variational framework ([Mielke and Roubíček, 2006](#)), the constitutive description of the damage model is based on

1. the *stored energy* functional

$$\mathcal{E}(\widehat{u}, \widehat{\omega}) = \mathcal{E}_{\text{std}}(\widehat{u}, \widehat{\omega}) + \mathcal{E}_{\text{reg}}(\widehat{\omega}) \quad (3)$$

with the *standard* part $\mathcal{E}_{\text{std}} : W^{1,2}(\Omega) \times \mathbb{Z} \rightarrow \mathbb{R}$ and the *regularizing* part $\mathcal{E}_{\text{reg}} : \mathbb{Z} \rightarrow \mathbb{R}$ respectively defined as

$$\mathcal{E}_{\text{std}}(\widehat{u}, \widehat{\omega}) = \frac{1}{2} \int_{\Omega} (1 - \widehat{\omega}(x)) E \widehat{u}'^2(x) \, dx \quad (4)$$

$$\mathcal{E}_{\text{reg}}(\widehat{\omega}) = \frac{1}{2} \int_{\Omega} g_{f0} \ell_0^2 \widehat{\omega}'^2(x) \, dx \quad (5)$$

where \widehat{u}' corresponds to an admissible strain field $\widehat{\varepsilon}$,

2. the *dissipation distance* $\mathcal{D} : \mathbb{Z} \times \mathbb{Z} \rightarrow \mathbb{R} \cup \{+\infty\}$

$$\mathcal{D}(\widehat{\omega}_1, \widehat{\omega}_2) = \begin{cases} \int_{\Omega} g_{f0} (\widehat{\omega}_2(x) - \widehat{\omega}_1(x)) \, dx & \text{if } \widehat{\omega}_2 \geq \widehat{\omega}_1 \text{ in } \Omega \\ +\infty & \text{otherwise} \end{cases} \quad (6)$$

Physically, \mathcal{E} represents the energy reversibly stored in the system and \mathcal{D} is the energy dissipated by changing the damage field from $\widehat{\omega}_1$ to $\widehat{\omega}_2$. The reversibly stored energy consists of the standard part \mathcal{E}_{std} and the regularizing part \mathcal{E}_{reg} ; the latter depends on the damage gradient and acts as a localization limiter. Note that \mathcal{E}_{reg} vanishes for uniform damage states. In Eqs. (4)–(6), E [Pa] denotes the Young modulus, g_{f0} [Jm^{-3}] is the amount of energy needed to disintegrate a unit volume of the material, and ℓ_0 [m] is a characteristic material length, which reflects the size and spacing of dominant heterogeneities in the microstructure. Later it will

become clear that the “ $+\infty$ ” term appearing in Eq. (6) enforces irreversibility of damage evolution, i.e., ensures that the damage variable cannot decrease in time.

Now, given the Dirichlet loading u_D , functionals \mathcal{E} and \mathcal{D} and initial data $\bar{u}_0 \in \mathbb{K}(0)$ and $\bar{\omega}_0 \in \mathbb{Z}$, the *energetic solution* of the damage problem is provided by time-dependent fields $u(t) \in \mathbb{K}(t)$ and $\omega(t) \in \mathbb{Z}$ satisfying (Mielke, 2005):

Global stability: for all $t \in [0; T]$, $\hat{u} \in \mathbb{K}(t)$ and $\hat{\omega} \in \mathbb{Z}$

$$\mathcal{E}(u(t), \omega(t)) \leq \mathcal{E}(\hat{u}, \hat{\omega}) + \mathcal{D}(\omega(t), \hat{\omega}) \quad (7)$$

Energy equality: for all $t \in [0; T]$

$$\mathcal{E}(u(t), \omega(t)) + \text{Var}_{\mathcal{D}}(\omega, [0; t]) = \mathcal{E}(u(0), \omega(0)) + \int_0^t \int_{\Gamma} R(s) \dot{u}_D(s) \, d\Gamma \, ds \quad (8)$$

where

$$\text{Var}_{\mathcal{D}}(\omega, [0; t]) = \sup \sum_{j=1}^J \mathcal{D}(\omega(t_{j-1}), \omega(t_j))$$

is the energy dissipated during the time interval $[0; t]$ (with the supremum taken over all partitions of $[0; t]$ in the form $0 = t_0 < t_1 < \dots < t_{J-1} < t_J = t$), R are the reactions arising at the boundary, and the product $R \dot{u}_D$ is the external power.

Initial conditions:

$$u(0) = \bar{u}_0 \quad \text{and} \quad \omega(0) = \bar{\omega}_0 \quad (9)$$

For simplicity, we will consider initial data $\bar{u}_0 = u_D(0) = 0$ and $\bar{\omega}_0 = 0$, which correspond to an initial undeformed and damage-free state. Note that, for initial conditions in such a form, the first term on the right-hand side of Eq. (8) vanishes and can be dropped.

Although conditions (7)–(9) present a formal definition of the energetic solution, the actual analysis will be performed using the time discretization technique, see e.g. Rektorys (1982) for a nice exposition. To that end, we consider a partition of the time interval $[0; T]$

$$0 = t_0 < t_1 = t_0 + \Delta t_1 < \dots < t_{N-1} + \Delta t_N = t_N = T \quad (10)$$

and recursively solve the minimization problem

$$(u_k, \omega_k) \in \text{Arg} \min_{(\hat{u}, \hat{\omega}) \in \mathbb{K}(t_k) \times \mathbb{Z}} [\mathcal{E}(\hat{u}, \hat{\omega}) + \mathcal{D}(\omega_{k-1}, \hat{\omega})] \quad \text{for } k = 1, 2, \dots, N \quad (11)$$

Here, e.g. u_k and ω_k abbreviate $u(t_k)$ and $\omega(t_k)$, and Argmin denotes the set of (possibly non-unique) minimizers of the incremental problem.

The main asset of the energetic solution concept is that, under reasonable data qualification, the solutions of the time-discretized problem converge to the energy-conserving energetic solution as $\max_k \Delta t_k \rightarrow 0$, see [Mielke and Roubíček \(2006\)](#); [Bouchitté et al. \(2009\)](#); [Mielke et al. \(2010\)](#); [Thomas and Mielke \(2010\)](#); [Mielke \(2011a\)](#). This convergence, however, requires the minimization in the stability condition (7) and the incremental problem (11) to be performed *globally*, implying that damage may initiate and propagate *before* the energy threshold g_{f0} is exceeded at any point of the structure—a phenomenon that is often found difficult to justify from the physical point of view. More physical, but also more technically involved, solution concepts thus rely on a suitable *local* energy minimization, see e.g. the overviews ([Mielke, 2011b](#); [Braides, 2014](#)) for the treatment of general rate-independent systems and ([Roubíček, 2015](#); [Vodička et al., 2014](#)) for damage- and delamination-related studies.

The approach we adopt here follows the earlier work by [Pham and Marigo \(2013\)](#) and consists of two adjustments to the introduced setting. First, we search for *critical points* of the incremental problem, corresponding to the so-called first-order stability conditions according to the terminology introduced in ([Pham and Marigo, 2013](#), Section 2). Second, once the threshold g_{f0} is reached for at least one point within the structure, the evolution is driven by the maximum of *damage variable* ω ; the Dirichlet data u_D are then obtained to be compatible with the resulting damage profiles, see ([Pham and Marigo, 2013](#), Section 4). As a result, we obtain solutions that are smooth in time and automatically satisfy the energy equality (8), ([Pham and Marigo, 2013](#), Property 1). Note that issues of local stability of the localized solutions and the relation between the present results and the alternative solution concepts are out of the scope of this paper and will be investigated separately.

3. Analysis of localization behavior

Having introduced the essentials of the variational framework, we will now proceed towards the main goal of this contribution – localization analysis of a simple uniaxial tensile test based on a critical point of the incremental variational principle (11), formulated for the time interval $[t_{k-1}; t_k]$.

3.1. Regularity study

The necessary optimality conditions of problem (11) read

$$\int_{\Omega} [\delta u'(x)(1 - \omega_k(x))Eu'_k(x) - \frac{1}{2}\delta\omega(x)Eu_k'^2(x) + \delta\omega'(x)g_{f0}\ell_0^2\omega'_k(x) + \delta\omega(x)g_{f0}] dx \geq 0 \quad (12)$$

for all admissible displacement variations $\delta u \in W^{1,2}(\Omega)$ vanishing on Γ and for arbitrary damage variations $\delta\omega \in W^{1,2}(\Omega)$ satisfying

$$\omega_{k-1}(x) \leq \omega_k(x) + \delta\omega(x) \leq 1 \text{ for } x \in \Omega \quad (13)$$

After integration by parts, we formally obtain¹

$$\begin{aligned} & - \int_{\Omega} \delta u(x) \left((1 - \omega_k(x)) E u'_k(x) \right)' dx - \int_{\Omega} \delta\omega(x) \left(\frac{1}{2} E u_k'^2(x) + g_{f0} \ell_0^2 \omega_k''(x) - g_{f0} \right) dx \\ & - \sum_i \llbracket \delta u(x) \left((1 - \omega_k(x)) E u'_k(x) \right) \rrbracket_{x_i} - \sum_j \llbracket \delta\omega(x) g_{f0} \ell_0^2 \omega_k'(x) \rrbracket_{x_j} + [\delta\omega(x) g_{f0} \ell_0^2 \omega_k'(x)]_{\Gamma} \geq 0 \end{aligned} \quad (14)$$

where

$$\llbracket f(x) \rrbracket_{x_i} = \lim_{x \rightarrow x_i^+} f(x) - \lim_{x \rightarrow x_i^-} f(x) \quad (15)$$

denotes the jump of function f at its discontinuity point x_i , and $[f(x)]_{\Gamma} = f(L/2) - f(-L/2)$. The sums in Eq. (14) are taken over all discontinuity points of arguments in the double brackets, if such discontinuities exist.

The arbitrariness of variations δu and their continuity give rise to conditions

$$\left((1 - \omega_k(x)) E u'_k(x) \right)' = 0 \text{ for } x \in \Omega, \quad \llbracket (1 - \omega_k(x)) E u'_k(x) \rrbracket_{x_i} = 0 \quad (16)$$

so that the stress, defined as $\sigma_k(x) = (1 - \omega_k(x)) E u'_k(x)$, remains constant along the whole bar:

$$(1 - \omega_k(x)) E u'_k(x) = \sigma_k = \text{const.} \quad (17)$$

Since the displacement derivative $u'_k(x)$ has the physical meaning of strain, it will be occasionally denoted as $\varepsilon_k(x)$.

It will be convenient for the forthcoming discussion to decompose the domain Ω at each time t_k into three disjoint sets²

$$\Omega_{e,k} = \{x \in \Omega : \omega_{k-1}(x) = \omega_k(x) < 1\} \quad (18)$$

$$\Omega_{d,k} = \{x \in \Omega : \omega_{k-1}(x) < \omega_k(x) < 1\} \quad (19)$$

$$\Omega_{f,k} = \{x \in \Omega : \omega_{k-1}(x) < \omega_k(x) = 1\} \quad (20)$$

¹Here, we need to assume that the solutions u and ω are piecewise C^2 continuous in Ω . Also note that u , ω , δu , and $\delta\omega$ are continuous functions on Ω , by virtue of the embedding $W^{1,2}(\Omega) \subset C^0(\bar{\Omega})$.

²It is not necessary to consider the case when $\omega_{k-1}(x) = \omega_k(x) = 1$. As soon as the damage reaches 1 at one point (cross section), no force can be transmitted by the bar and the failure process is complete.

corresponding to the elastic, damaging and fully damaged regions, respectively. Note that the elastic region is understood as the region with a vanishing damage *increment* between t_{k-1} and t_k , not necessarily with a vanishing damage *value*. In order to meet the admissibility condition (13), the variation $\delta\omega(x)$ can only be non-negative for $x \in \Omega_{e,k}$, non-positive for $x \in \Omega_{f,k}$, and of an arbitrary sign for $x \in \Omega_{d,k}$. Therefore, the Karush-Kuhn-Tucker optimality conditions, e.g. (Jahn, 2007, Section 5.2), with respect to $\delta\omega$, implied by Eq. (14), read

$$g_{f0}\ell_0^2\omega_k''(x) + \frac{1}{2}Eu_k^2(x) \leq g_{f0}, \quad \llbracket\omega_k'(x)\rrbracket_{x_j} \leq 0 \quad \text{for } x, x_j \in \Omega_{e,k} \quad (21)$$

$$g_{f0}\ell_0^2\omega_k''(x) + \frac{1}{2}Eu_k^2(x) = g_{f0}, \quad \llbracket\omega_k'(x)\rrbracket_{x_j} = 0 \quad \text{for } x, x_j \in \Omega_{d,k} \quad (22)$$

$$g_{f0}\ell_0^2\omega_k''(x) + \frac{1}{2}Eu_k^2(x) \geq g_{f0}, \quad \llbracket\omega_k'(x)\rrbracket_{x_j} \geq 0 \quad \text{for } x, x_j \in \Omega_{f,k} \quad (23)$$

In addition, at the boundary $\Gamma = \{-L/2, L/2\}$ we obtain

$$\omega_k'(-L/2) = 0, \quad \omega_k'(L/2) = 0 \quad (24)$$

If a boundary point belongs to $\Omega_{d,k}$, the condition of vanishing derivative ω_k' can be directly deduced from variational inequality (14), using the argument that the variation $\delta\omega$ can have an arbitrary sign. If, on the other hand, a boundary point belongs to $\Omega_{e,k}$, then the variation $\delta\omega$ at that point is nonnegative and (14) implies $\omega_k'(-L/2) \leq 0$ at the left boundary, or $\omega_k'(L/2) \geq 0$ at the right boundary. But even then the derivative must vanish, as can be shown by contradiction. Initially, damage is identically zero in the whole bar and the condition of zero derivative at the boundary is satisfied. Suppose that k is the first step in which $\omega_k'(-L/2)$ becomes negative. Since the boundary point $-L/2$ must belong to $\Omega_{e,k}$ (otherwise the first condition in (24) would apply by virtue of (14)), the damage increment at that point must be zero and $\omega_k(-L/2) = \omega_{k-1}(-L/2)$. But then $\omega_k'(-L/2)$ cannot be smaller than $\omega_{k-1}'(-L/2)$ without violating the condition that the damage increments must not be negative. Since $\omega_{k-1}'(-L/2) = 0$, we conclude that $\omega_k'(-L/2)$ cannot be negative. Similar arguments (just with the opposite inequalities) can be used at the right boundary. This proves that homogeneous Neumann boundary conditions (24) are universally applicable, independently of the state of the material at the boundary.

3.2. Elastic response

According to Eq. (9) with the standard initial values $\bar{u}_0 = 0$ and $\bar{\omega}_0 = 0$, the loading program is assumed to start from an initial undeformed and damage-free state, and so $u_0(x) = 0$, $\varepsilon_0(x) = u_0'(x) = 0$, $\omega_0(x) = 0$ and $\sigma_0 = 0$. The first condition in (21) is then satisfied as a strict inequality and the entire bar is in an elastic state, $\Omega_{e,0} = \Omega$. As the applied displacement at the boundary is increased,

the bar deforms and, up to a certain level of loading, remains elastic. As long as the damage remains zero, Eq. (17) implies that

$$\varepsilon_k(x) \equiv u'_k(x) = \frac{\sigma_k}{E} \quad (25)$$

where σ_k is the current stress level. This means that, before the onset of damage, the strain is uniform. Such a solution remains admissible as long as the first part of (21) is satisfied. In view of Eq. (25), this condition can be rewritten as

$$\frac{\sigma_k^2}{2E} \leq g_{f0} \quad (26)$$

The stress level can be linked to the applied displacements at the boundary, since the bar elongation (change of length) is given by

$$e_k = \int_{\Omega} \varepsilon_k(x) dx = \frac{\sigma_k}{E} \int_{\Omega} dx = \frac{\sigma_k L}{E} \quad (27)$$

The onset of damage is attained when Eq. (26) is satisfied as an equality, i.e., when

$$\sigma_k = \sqrt{2Eg_{f0}} \equiv f_t \quad (28)$$

where f_t denotes the tensile strength, derived from the given elastic modulus E and parameter g_{f0} . The corresponding bar elongation at the onset of damage is

$$e_{od} = \frac{f_t L}{E} \quad (29)$$

When the actual elongation exceeds this value, the bar cannot remain elastic along its entire length because condition (26) would be violated.

In what follows, the time corresponding to the onset of damage is referred to as t_{od} , and our objective is to characterize the response of the bar for $t_k \geq t_{od}$. In fact, since the elastic solution is described by very simple closed-form expressions, the loading process from the initial state to the onset of damage can be handled by a single increment and we can select time t_1 such that $e_1 = e_{od}$.

3.3. Damage evolution

When the damage threshold is exceeded, the strain field cannot remain uniform. According to Eq. (17), uniform strain would imply uniform damage, $\omega_k(x) = \text{const.}$, but then the first term on the left-hand side of Eq. (22) would vanish and the condition would reduce to

$$\frac{1}{2} E \varepsilon_k^2 = g_{f0} \quad (30)$$

which is satisfied exclusively for the state at the onset of damage.

In order to derive the governing equation for the damage field in the damaging zone $\Omega_{d,k}$, we divide Eq. (22) by g_{f0} and, employing identity (17), rewrite it in the form of a non-linear ordinary differential equation

$$\ell_0^2 \omega_k''(x) + \frac{\mu_k}{(1 - \omega_k(x))^2} = 1 \quad (31)$$

where the newly introduced dimensionless parameter

$$\mu_k = \frac{\sigma_k^2}{2Eg_{f0}} \quad (32)$$

provides a convenient parametrization to the damage evolution, as will be shown next. At the onset of damage, $\omega_1(x) = 0$, $\sigma_1 = f_t = \sqrt{2Eg_{f0}}$, and $\mu_1 = f_t^2/2Eg_{f0} = 1$.

Eq. (31) is an ordinary second-order differential equation, which should be satisfied in the unknown damaging zone $\Omega_{d,k}$, and as such it represents a *free-boundary problem*, e.g. (Friedman, 1982). Therefore, apart from the solution ω_k itself, we also search for the so-called *noncoincidence set* $\Omega_{d,k}$ and the continuity (or regularity) conditions at the *free-boundary* $\partial\Omega_{d,k}$ separating the damaging zone from the elastic zone. The advantage of the variational format of the model is that the optimality conditions (21)–(23) encode the appropriate conditions at the elastic-damaging interface.

In what follows, we assume that the damaging region is a single interval of length $L_{d,k}$ and that it is shorter than the entire bar (i.e., that $L_{d,k} < L$), to ensure that the physical boundary of the bar is located in the elastic region.³ However, for a perfectly uniform bar (i.e., a bar with constant cross-sectional area and constant material properties along the length) the solution would not be unique because the damage zone can be arbitrarily translated along the bar. Physically, the actual position of the damage zone would be determined by random imperfections. Without loss of generality, we can thus assume that the damage zone

$$\Omega_{d,k} = (-L_{d,k}/2; L_{d,k}/2) \quad (33)$$

is centered at the origin of the spatial coordinates. Note that $\Omega_{d,k}$ is an open interval, and the points $\pm L_{d,k}/2$ belong to $\Omega_{e,k}$.

For the right boundary of the damaging zone $\Omega_{d,k}$ (i.e., for the point $L_{d,k}/2$, which itself belongs to $\Omega_{e,k}$), we infer from the second part of (21) that

$$\lim_{x \rightarrow L_{d,k}^-/2} \omega_k'(x) \geq \lim_{x \rightarrow L_{d,k}^+/2} \omega_k'(x) \quad (34)$$

³Solutions localized at the boundary or in multiple non-overlapping damaging intervals can be treated using this basic scenario, as discussed in detail by Pham and Marigo (2013).

Let us first assume that the damage zone expands, i.e., that $L_{d,k} \geq L_{d,k-1} \geq \dots \geq L_{d,2}$ (the case of a contracting damage zone will be treated later, in Section 3.4). In this case, $\omega_k(x) = 0$ for all $x \geq L_{d,k}/2$ and the right-hand side of (34) vanishes. The condition then reduces to

$$\lim_{x \rightarrow L_{d,k}^-} \omega'_k(x) \geq 0 \quad (35)$$

Since the value of damage at point $L_{d,k}/2$ is zero and the values to the left of this point are nonnegative, the limit on the left-hand side of (35), which represents the derivative from the left, cannot be positive. Consequently, ω'_k must vanish at $x = L_{d,k}/2$, and by similar arguments we can show that it must also vanish at $x = -L_{d,k}/2$, which means that the solution preserves continuous differentiability.

In summary, the solution must satisfy conditions

$$\omega_k(-L_{d,k}/2) = \omega_k(L_{d,k}/2) = 0, \quad \omega'_k(-L_{d,k}/2) = \omega'_k(L_{d,k}/2) = 0 \quad (36)$$

These are the free-boundary conditions to be imposed on the solution of differential equation (31). In general one could consider the coordinates of the left and right boundary points of the damage zone as independent unknowns and conditions analogous to (36) would be used to determine these two unknowns plus two integration constants present in the general solution of Eq. (31). The assumed symmetry of the damaging zone, Eq. (33), implies that one of conditions (36) becomes redundant and the remaining three can be used to determine the size of the damage zone, $L_{d,k}$, and two integration constants. An interested reader is invited to consult Jirásek et al. (2013); Rokoš et al. (2015) for related results in the context of softening gradient plasticity with non-uniform data. Eq. (31) is nonlinear and cannot be solved in closed form. However, if we consider the state just at the onset of damage and rewrite the equation in the rate form, we obtain a linear equation that can be handled analytically. To this end, let us assume that the damage evolution is sufficiently smooth⁴ in time, such that we can introduce the damage rate

$$\dot{\omega}_k(x) = \lim_{\Delta t_{k+1} \rightarrow 0^+} \frac{\omega(t_{k+1}) - \omega(t_k)}{\Delta t_{k+1}}, \quad (37)$$

and rewrite Eq. (31) in the rate form as

$$\ell_0^2 \dot{\omega}_k''(x) + 2 \frac{\mu_k}{(1 - \omega_k(x))^3} \dot{\omega}_k(x) = - \frac{\dot{\mu}_k}{(1 - \omega_k(x))^2} \quad (38)$$

⁴Later it will be shown that, due to the regularizing energy term (5), the response of the bar is continuous despite the brittle character of the underlying non-regularized material model.

This is an ordinary linear second-order differential equation for the damage rate $\dot{\omega}_k$ with possibly non-constant coefficients. Recall that damage irreversibility requires $\dot{\omega}_k \geq 0$.

As already explained, at the onset of damage we have $\omega_1(x) = 0$ and $\mu_1 = 1$. Then, Eq. (38) further simplifies to

$$\ell_0^2 \dot{\omega}_1''(x) + 2\dot{\omega}_1(x) = -\dot{\mu}_1 \quad (39)$$

which has the general solution

$$\dot{\omega}_1(x) = -\frac{1}{2}\dot{\mu}_1 + C_1 \cos \frac{\sqrt{2}x}{\ell_0} + C_2 \sin \frac{\sqrt{2}x}{\ell_0}, \quad x \in \Omega_{d,2} \quad (40)$$

Here, C_1 and C_2 denote the integration constants, which should be determined from appropriate boundary conditions. Let us postulate these conditions by analogy with (36) in the form

$$\dot{\omega}_1(-L_{d,2}/2) = \dot{\omega}_1(L_{d,2}/2) = 0, \quad \dot{\omega}_1'(-L_{d,2}/2) = \dot{\omega}_1'(L_{d,2}/2) = 0 \quad (41)$$

Substituting the general solution (40) into (41), we obtain integration constants

$$C_1 = -\frac{1}{2}\dot{\mu}_1, \quad C_2 = 0 \quad (42)$$

as well as the initial size of the damage zone

$$L_{d,2} = \sqrt{2}\pi\ell_0 \quad (43)$$

The rate of the damage variable at the onset of damage, plotted in Figure 2(a), is therefore given by

$$\dot{\omega}_1(x) = -\frac{1}{2}\dot{\mu}_1 \left(1 + \cos \frac{\sqrt{2}x}{\ell_0} \right) \quad \text{for } x \in \Omega_{d,2} \quad (44)$$

This is consistent with the damage irreversibility constraint $\dot{\omega}_1 \geq 0$ only if $\dot{\mu}_1 < 0$, which corresponds to a negative stress rate (the case of $\dot{\mu}_1 = 0$ can be excluded because it can occur only if the state of the bar does not change at all and all variables remain constant in time). Consequently, the onset of damage immediately results into a *softening* response.

3.4. Numerical solution

Eq. (44) describes the initial damage rate at the onset of localization, but the damage profiles at later stages of the failure process should be solved from Eq. (31). Since the analytical solution is not available, we resort to a numerical procedure

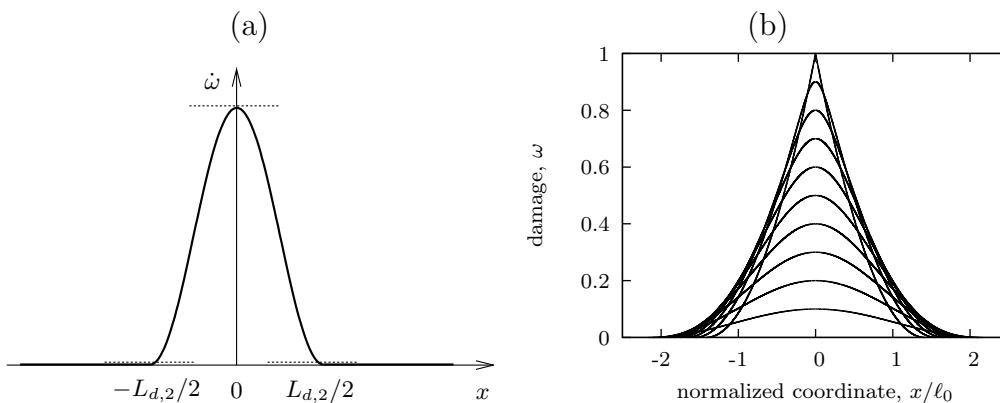


Figure 2: (a) Sketch of the damage rate profile at the onset of damage; (b) inadmissible evolution of the damage profile computed using conditions (36) in terms of the total damage ($\omega = 0$ and $\omega' = 0$ at the boundary of the damage zone).

using a variant of the shooting method, the details of which are given in [Appendix A](#).

Let us recall that the derivation of boundary conditions (36) was based on the assumption that the damage zone expands and thus is always surrounded by an undamaged material. Numerically constructed damage profiles obtained by solving Eq. (31) with conditions (36) are plotted in Figure 2(b). The solution of the first inelastic step is admissible and agrees well with the analytical result (44). In subsequent steps the size of the damage zone L_d tends to decrease, but then the numerically computed damage would, at some points near the boundary of the damage zone, decrease as well, which violates the damage irreversibility constraint. Such solutions are inadmissible and conditions (36) need to be revisited.

If $L_{d,k} < L_{d,k-1}$, then the damage at the boundary of $\Omega_{d,k}$ is not zero—it should be equal to the value after the previous step. This can be described by conditions

$$\omega_k(-L_{d,k}/2) = \omega_{k-1}(-L_{d,k}/2), \quad \omega_k(L_{d,k}/2) = \omega_{k-1}(L_{d,k}/2) \quad (45)$$

For the spatial derivative of damage at $x = L_{d,k}/2$, we can again use condition (34) derived from the variational inequality (14), taking into account that $\omega_k(x) = \omega_{k-1}(x)$ for all $x \geq L_{d,k}/2$. Consequently, (34) can be rewritten as

$$\lim_{x \rightarrow L_{d,k}^-} \omega'_k(x) \geq \omega'_{k-1}(L_{d,k}/2) \quad (46)$$

However, since $\omega_k(L_{d,k}/2) = \omega_{k-1}(L_{d,k}/2)$ and $\omega_k(x) \geq \omega_{k-1}(x)$ for all $x < L_{d,k}/2$, condition (46) can be satisfied only as an equality, and the damage profile remains continuously differentiable. Analogous arguments can be used at the left boundary of the damage zone. The resulting conditions for the derivative of damage are

$$\omega'_k(-L_{d,k}/2) = \omega'_{k-1}(-L_{d,k}/2), \quad \omega'_k(L_{d,k}/2) = \omega'_{k-1}(L_{d,k}/2) \quad (47)$$

Imposing conditions (47) combined with (45), we obtain an admissible damage evolution shown in Figure 3, in which the size of the active part of the damage zone is decreasing in time but the irreversibility constraint is satisfied and previously generated damage does not decrease at any point. The solutions also meet the C^1 continuity inside the damaged region, Eq. (22), even for high values of damage. The plotted profiles correspond to values of maximum damage ω_{\max} ranging from 0.1 to 0.9 with step 0.1, but they have been constructed by an incremental numerical procedure with a much smaller step size, making sure that the numerical error is negligible.

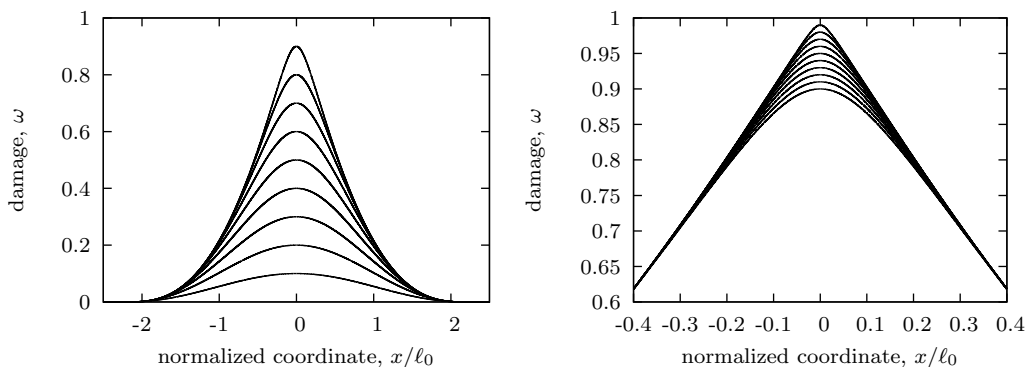


Figure 3: Evolution of damage profile computed using conditions (45) and (47) in terms of the damage increment ($\Delta\omega = 0$ and $\Delta\omega' = 0$ at the boundary of the damage zone), plotted (a) for maximum damage ω_{\max} between 0.1 and 0.9, (b) for maximum damage ω_{\max} between 0.9 and 0.99.

Interestingly, conditions (45) and (47) can be rewritten in terms of the damage increments as

$$\Delta\omega_k(-L_{d,k}/2) = \Delta\omega_k(L_{d,k}/2) = 0 \quad (48)$$

$$\Delta\omega'_k(-L_{d,k}/2) = \Delta\omega'_k(L_{d,k}/2) = 0 \quad (49)$$

and they remain applicable even if the damage zone expands. However, if the problem is considered in the rate form, it is not always correct to construct the appropriate conditions simply by replacing the damage increment by damage rate. To gain more insight into the conditions that describe an evolving boundary between the (active) damage zone and the zone of elastic unloading, let us consider an incremental step from t_k to $t_{k+1} = t_k + \Delta t$ and let us express the computed damage zone size at the end of the step as $L_{d,k+1}(\Delta t)$, marking explicitly that it depends on the size of the step. In a similar spirit, the computed damage at the end of the step can be denoted as $\omega_{k+1}(x, \Delta t)$.

In the case of an *expanding* damage zone, the solution satisfies conditions (36), which can now be rewritten as

$$\omega_{k+1}(L_{d,k+1}(\Delta t)/2, \Delta t) = 0 \quad (50)$$

$$\omega'_{k+1}(L_{d,k+1}(\Delta t)/2, \Delta t) = 0 \quad (51)$$

Since these conditions are satisfied for any step size Δt , we can differentiate with respect to Δt and evaluate the derivative at $\Delta t = 0$, which yields

$$\omega'_k(L_{d,k}/2)\dot{L}_{d,k+1}(0)/2 + \dot{\omega}_k(L_{d,k}/2) = 0 \quad (52)$$

$$\omega''_k(L_{d,k}/2)\dot{L}_{d,k+1}(0)/2 + \dot{\omega}'_k(L_{d,k}/2) = 0 \quad (53)$$

Since $\omega'_k(L_{d,k}/2) = 0$, condition (52) implies $\dot{\omega}_k(L_{d,k}/2) = 0$. On the other hand, $\omega''_k(L_{d,k}/2)$ is zero only for $k = 1$; in general it is equal to $(1 - \mu_k)/\ell_0^2$, as follows from Eq. (31). Therefore, it was correct to use conditions (41) for the initial damage rate just at the onset of damage, but for $k > 1$ we have $\mu_k < 1$ and $\omega''_k(L_{d,k}/2) = (1 - \mu_k)/\ell_0^2 > 0$. Condition (53) can then be used to express the rate of the damage zone size as

$$\dot{L}_{d,k+1}(0) = -\frac{2\ell_0^2\dot{\omega}'_k(L_{d,k}/2)}{1 - \mu_k} \quad (54)$$

As we can see, $\dot{\omega}'_k(L_{d,k}/2)$ would not be zero if the damage zone truly expanded. But for a *contracting* damage zone we have to use conditions (45) and (47), and then (50)–(51) is replaced by

$$\omega_{k+1}(L_{d,k+1}(\Delta t)/2, \Delta t) = \omega_k(L_{d,k+1}(\Delta t)/2) \quad (55)$$

$$\omega'_{k+1}(L_{d,k+1}(\Delta t)/2, \Delta t) = \omega'_k(L_{d,k+1}(\Delta t)/2) \quad (56)$$

and differentiation with respect to Δt yields

$$\omega'_k(L_{d,k}/2)\dot{L}_{d,k+1}(0)/2 + \dot{\omega}_k(L_{d,k}/2) = \omega'_k(L_{d,k}/2)\dot{L}_{d,k+1}(0)/2 \quad (57)$$

$$\omega''_k(L_{d,k}/2)\dot{L}_{d,k+1}(0)/2 + \dot{\omega}'_k(L_{d,k}/2) = \omega''_k(L_{d,k}/2)\dot{L}_{d,k+1}(0)/2 \quad (58)$$

which implies

$$\dot{\omega}_k(L_{d,k}/2) = 0, \quad \dot{\omega}'_k(L_{d,k}/2) = 0 \quad (59)$$

This means that, in the case of a contracting zone, conditions (41) can be used for any k .

After this detailed discussion of conditions imposed at the evolving boundary of the damage zone, let us turn our attention back to the numerically computed solution of Eq. (31). The damage profiles from Figure 3 are complemented by the evolution of strain profiles obtained from Eq. (17) and normalized by the limit elastic strain, $\varepsilon_0 = \sqrt{2g_{f0}/E}$; see Figure 4. The results confirm that not only damage but also strain tends to localize into a contracting zone, while the strains in the elastically unloading zones are decreasing.

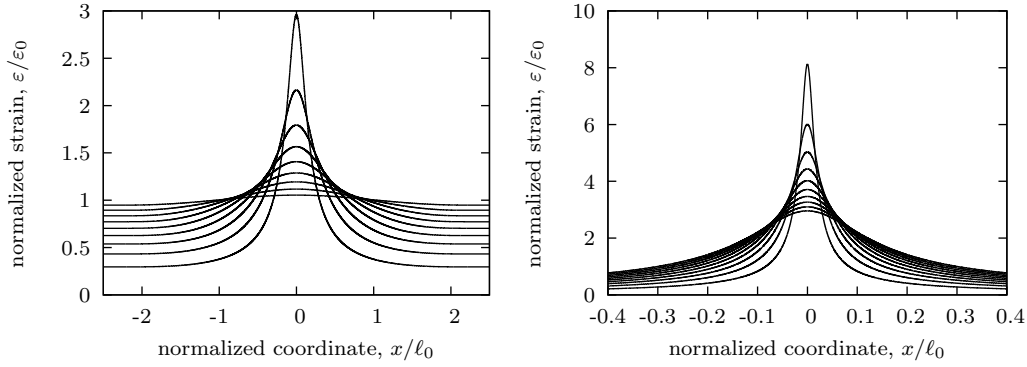


Figure 4: Evolution of strain profile computed using conditions (45) and (47) in terms of the damage increment ($\Delta\omega = 0$ and $\Delta\omega' = 0$), plotted (a) for maximum damage ω_{\max} between 0.1 and 0.9, (b) for maximum damage ω_{\max} between 0.9 and 0.99.

In order to assess the implication of the strain localization at the structural level, we also characterize the response by the inelastic part of the elongation, obtained as

$$\begin{aligned}
 w_k &= \int_{-L/2}^{L/2} \left(\varepsilon_k(x) - \frac{\sigma_k}{E} \right) dx = \int_{-L/2}^{L/2} \left(\frac{\sigma_k}{E(1 - \omega_k(x))} - \frac{\sigma_k}{E} \right) dx = \\
 &= \frac{\sigma_k}{E} \int_{-L/2}^{L/2} \frac{\omega_k(x)}{1 - \omega_k(x)} dx = \frac{\sigma_k}{E} \int_{-L_{d,\max}/2}^{L_{d,\max}/2} \frac{\omega_k(x)}{1 - \omega_k(x)} dx
 \end{aligned} \tag{60}$$

where $L_{d,\max}$ is the maximum size of the damage zone ever reached in the previous history (in the present case of a contracting zone it is equal to $L_{d,2}$). Again, a dimensionless representation is used, in which the inelastic displacement is normalized by $\ell_0\varepsilon_0$ and the stress σ_k is divided by the tensile strength, $f_t = \sqrt{2Eg_{f0}}$. The normalized diagram in Figure 5(a) reveals that the inelastic displacement reaches its maximum after softening to $\approx 40\%$ of the peak stress and then decreases to zero. In terms of the structural response, represented by the diagram of stress versus total elongation, this leads to a strong snapback; see Figure 5(b). The total elongation is easily expressed as

$$u_k = \int_{-L/2}^{L/2} \varepsilon_k(x) dx = w_k + \frac{\sigma_k L}{E} \tag{61}$$

and in Figure 5(b) it is normalized by $\ell_0\varepsilon_0$. Of course, snapback at the structural level can always be expected for very long bars, but here it occurs for short bars, too. The diagram has been plotted for the total bar length set to $L = 5\ell_0$, which is only slightly larger than the initial damage zone size $L_{d,2} = \sqrt{2}\pi\ell_0 \approx 4.443\ell_0$.

Shrinking of the damage zone is further documented in Figure 6, which shows the evolution of L_d and demonstrates that, at complete failure, the active zone

degenerates to a point. It is interesting to observe that when the (incorrect) boundary conditions in terms of the total damage are applied, the damaging zone is substantially larger and is of a non-zero length at failure; see the dashed curve in Figure 5(b). Still, this phenomenon has limited effect on the structural response, and is not strong enough to eliminate the snapback phenomenon; see the dashed curves in Figure 5.

In the following sections, we shall investigate to which extent such behavior can be influenced by more advanced constitutive models. To avoid a profusion of notation, the indices referring to a given time step are omitted in what follows.

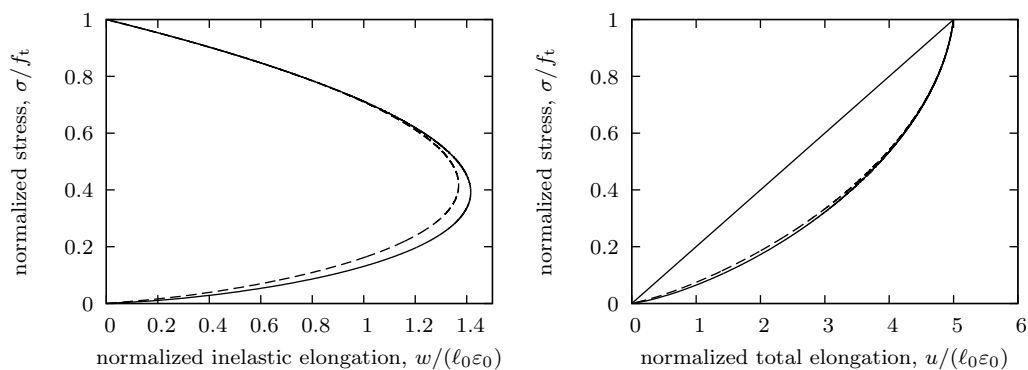


Figure 5: Relation between stress and (a) inelastic part of elongation, (b) total elongation (for a bar of total length $L = 5\ell_0$); solid curves correspond to conditions (45) and (47) in terms of the damage increment ($\Delta\omega = 0$ and $\Delta\omega' = 0$), dashed curves to conditions (36) in terms of the total damage ($\omega = 0$ and $\omega' = 0$).

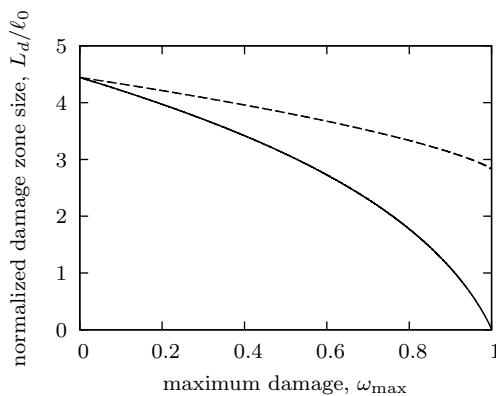


Figure 6: Evolution of the size of damage zone as a function of maximum damage; solid curves correspond to conditions (45) and (47) in terms of the damage increment ($\Delta\omega = 0$ and $\Delta\omega' = 0$), dashed curves to conditions (36) in terms of the total damage ($\omega = 0$ and $\omega' = 0$).

4. Generalized formulation with softening

4.1. Governing equations

The model considered in the previous section exhibits an extremely brittle behavior. This is related to the specific definition of the dissipation distance (6), which is motivated by the concept of an elastic-brittle response. In general it can be replaced by

$$\mathcal{D}(\widehat{\omega}_1, \widehat{\omega}_2) = \begin{cases} \int_{\Omega} (D(\widehat{\omega}_2(x)) - D(\widehat{\omega}_1(x))) \, dx & \text{if } \widehat{\omega}_2 \geq \widehat{\omega}_1 \text{ in } \Omega \\ +\infty & \text{otherwise} \end{cases} \quad (62)$$

where D is a function that represents the density of energy dissipated in a damage process up to a given damage level. This function should be non-decreasing, with $D(0) = 0$ and $D(1) = g_{f\infty}$ = density of energy dissipated by the complete failure process.

To construct simple but physically meaningful forms of function D , let us consider the idealized case of uniform damage, such that the regularizing part of stored energy remains equal to zero. The stored energy then reduces to the standard part (4), which can be rewritten as

$$\mathcal{E}_{\text{std}}(\widehat{u}, \widehat{\omega}) = \int_{\Omega} \Psi(\widehat{u}'^2(x), \widehat{\omega}(x)) \, dx \quad (63)$$

where

$$\Psi(\varepsilon, \omega) = \frac{1}{2}(1 - \omega)E\varepsilon^2 \quad (64)$$

is the density of stored elastic energy (more precisely, of the Helmholtz free energy). The graphical meaning is illustrated in Figure 7. The vertically hashed area corresponds to the density of free energy and the horizontally hashed area is the density of dissipated energy, $D(\omega)$. Under isothermal conditions, their sum must be equal to the density of supplied work (all densities being taken per unit volume).

From the incremental energy balance equation

$$\frac{\partial \Psi}{\partial \varepsilon} d\varepsilon + \frac{\partial \Psi}{\partial \omega} d\omega + \frac{dD}{d\omega} d\omega = \sigma d\varepsilon \quad (65)$$

we get the stress-strain relation

$$\sigma = \frac{\partial \Psi}{\partial \varepsilon} = (1 - \omega)E\varepsilon \quad (66)$$

and an additional equation

$$\frac{dD}{d\omega} = -\frac{\partial \Psi}{\partial \omega} = \frac{1}{2}E\varepsilon^2 \quad (67)$$

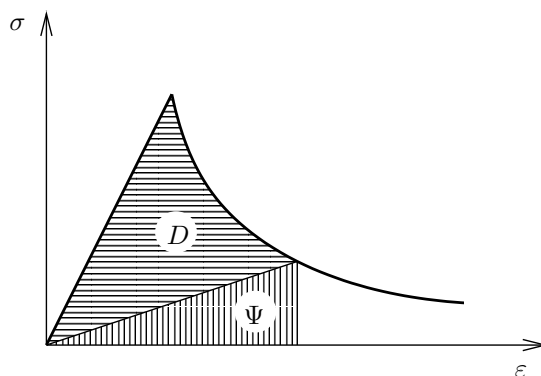


Figure 7: Stress-strain diagram (under uniform strain) and the meaning of free energy Ψ and dissipated energy D .

in which ε has to be understood as the strain that produced the current damage level ω . The negative derivative of free energy density with respect to the damage variable is called the damage energy release rate and denoted as Y .

Suppose that we would like to construct a model which, under uniform damage and monotonic loading, produces a specific shape of the stress-strain diagram, described by

$$\sigma = s(\varepsilon) \quad (68)$$

where s is a given function. To recover this stress-strain relation from the constitutive law of the damage model,

$$\sigma = (1 - \omega)E\varepsilon \quad (69)$$

we need to consider the damage variable as a function of the current strain (still assuming monotonic loading) and postulate a damage law in the form

$$\omega = 1 - \frac{s(\varepsilon)}{E\varepsilon} \equiv g(\varepsilon) \quad (70)$$

In this way, the damage function g can be constructed directly from the given shape of the stress-strain diagram. In the interval of growing damage (i.e., above the damage threshold and below the state of complete damage), the damage law is invertible and the strain ε corresponding to a given damage level ω can be expressed as

$$\varepsilon = g^*(\omega) \quad (71)$$

where g^* is the inverse function of g . Recall that the damage energy release rate, $-\partial\Psi/\partial\omega$, has been denoted as Y . Consequently, Eq. (67) can be rewritten as

$$\frac{dD(\omega)}{d\omega} = Y(\omega) = \frac{1}{2}Eg^{*2}(\omega) \quad (72)$$

By integrating this relation, we can construct an appropriate formula for the dissipation density function

$$D(\omega) = \int_0^\omega Y(\tilde{\omega}) d\tilde{\omega} = \frac{1}{2}E \int_0^\omega g^{*2}(\tilde{\omega}) d\tilde{\omega} \quad (73)$$

Let us emphasize that Eqs. (65)–(73) apply to the local version of the damage model, with regularizing terms omitted. For such a local model, the local values of strain and damage at a given point are, during damage growth, directly linked by Eq. (70). However, for a model regularized by the energy term dependent on the damage gradient, the analysis from Section 3 must be repeated with an appropriate modification—the term $\delta\omega(x)g_{f0}$ in Eq. (12) is replaced by $\delta\omega(x)Y(\omega(x))$ while the regularizing term remains unchanged. The modified form of Eq. (14) is then

$$\begin{aligned} & - \int_{\Omega} \delta u(x) \left((1 - \omega(x)) E u'(x) \right)' dx - \\ & - \int_{\Omega} \delta\omega(x) \left(\frac{1}{2} E u'^2(x) + g_{f0} \ell_0^2 \omega''(x) - Y(\omega(x)) \right) dx + \\ & + [\delta\omega(x) g_{f0} \ell_0^2 \omega'(x)]_{\Gamma} \geq 0 \end{aligned} \quad (74)$$

Inside the damage zone, the variation $\delta\omega(x)$ is arbitrary and the resulting optimality condition

$$\frac{1}{2} E u'^2(x) + g_{f0} \ell_0^2 \omega''(x) - Y(\omega(x)) = 0 \quad (75)$$

has the form of a differential equation. Repeating the procedure from Section 3.3, we can convert it into

$$\ell_0^2 \omega''(x) + \frac{\mu}{(1 - \omega(x))^2} = \frac{Y(\omega(x))}{g_{f0}} \quad (76)$$

which is the generalized form of Eq. (31), to be used in subsequent analyses. However, it is also instructive to look at another interpretation of Eq. (75). Taking into account Eq. (72) and denoting u' as ε , we can rewrite Eq. (75) as

$$\varepsilon^2(x) = g^{*2}(\omega(x)) - \frac{2g_{f0}}{E} \ell_0^2 \omega''(x) \quad (77)$$

This is a differential relation between strain and damage that is valid inside the damage zone and replaces the algebraic relation (71). Since $\sqrt{2g_{f0}/E} = \varepsilon_0 =$ limit elastic strain, we can further rewrite Eq. (77) as

$$\varepsilon(x) = \sqrt{g^{*2}(\omega(x)) - \varepsilon_0^2 \ell_0^2 \omega''(x)} \quad (78)$$

or, in the inverse form, as

$$\omega(x) = g \left(\sqrt{\varepsilon^2(x) + \varepsilon_0^2 \ell_0^2 \omega''(x)} \right) \quad (79)$$

The last relation is a generalized form of Eq. (70). It shows that the regularizing term accelerates the damage growth (as compared to the local model) in regions where the current damage profile is convex ($\omega''(x) > 0$) and decelerates it in regions where the current damage profile is concave ($\omega''(x) < 0$). This, combined with continuity of damage, prevents the damage profile from becoming “too much localized”.

4.2. Model with linear softening

The simplest description of a stress-strain law with softening is based on the linear relation between stress and strain in the post-peak range, from the limit elastic strain ε_0 to a certain failure strain ε_f , which must not be smaller than ε_0 . The special case of $\varepsilon_f = \varepsilon_0$ corresponds to the brittle model considered in the previous section, and for increasing ε_f we obtain a more ductile behavior. Therefore, the dimensionless ratio

$$\beta = \frac{\varepsilon_0}{\varepsilon_f} \quad (80)$$

which is between 0 and 1, can be called the brittleness number.

The softening branch of the stress-strain diagram with linear softening is described by

$$\sigma = s(\varepsilon) \equiv E\varepsilon_0 \frac{\varepsilon_f - \varepsilon}{\varepsilon_f - \varepsilon_0}, \quad \varepsilon_0 \leq \varepsilon \leq \varepsilon_f \quad (81)$$

and the corresponding damage function evaluated according to Eq. (70) is

$$g(\varepsilon) = 1 - \frac{s(\varepsilon)}{E\varepsilon} = 1 - \frac{\varepsilon_0}{\varepsilon} \cdot \frac{\varepsilon_f - \varepsilon}{\varepsilon_f - \varepsilon_0} = \frac{(\varepsilon - \varepsilon_0)\varepsilon_f}{(\varepsilon_f - \varepsilon_0)\varepsilon} = \frac{1}{1 - \beta} \left(1 - \frac{\varepsilon_0}{\varepsilon} \right), \quad \varepsilon_0 \leq \varepsilon \leq \varepsilon_f \quad (82)$$

In this simple case, the inverse function can be evaluated analytically as

$$g^*(\omega) = \frac{\varepsilon_0}{1 - \omega + \beta\omega}, \quad 0 \leq \omega \leq 1 \quad (83)$$

and after substitution into (72)–(73) we get

$$Y(\omega) = \frac{1}{2} E g^{*2}(\omega) = \frac{1}{2} E \frac{\varepsilon_0^2}{(1 - \omega + \beta\omega)^2} = \frac{g_f \varepsilon_0}{(1 - \omega + \beta\omega)^2} \quad (84)$$

$$D(\omega) = \int_0^\omega Y(\tilde{\omega}) d\tilde{\omega} = \frac{g_f \varepsilon_0}{1 - \beta} \left(\frac{1}{1 - \omega + \beta\omega} - 1 \right) \quad (85)$$

For $\omega = 1$, the last expression gives

$$g_{f\infty} = D(1) = \frac{g_{f0}}{1-\beta} \left(\frac{1}{\beta} - 1 \right) = \frac{g_{f0}}{\beta} \quad (86)$$

Recall that $\beta = \varepsilon_0/\varepsilon_f =$ brittleness number between 0 and 1. The case of $\beta = 1$ corresponds to the elastic-brittle model from Section 4, smaller values correspond to a less brittle behavior, with $g_{f\infty} > g_{f0}$. Eq. (76), to be satisfied along the damage zone, is for the case of linear softening written as

$$\ell_0^2 \omega''(x) + \frac{\mu}{(1-\omega(x))^2} = \frac{1}{(1-\omega(x) + \beta\omega(x))^2} \quad (87)$$

The numerically evaluated evolution of the damage and strain profiles is shown in Figure 8 for $\beta = 0.5$ and in Figure 9 for $\beta = 0.1$. For a material with more ductile local response (lower brittleness number, Figure 9), the initial size of the damage zone is larger, but the active part of the damage zone is shrinking and tends to one single cross section of the bar as the maximum damage tends to 1. This is shown in Figure 10, in which the solid curve corresponds to the elastic-brittle model ($\beta = 1$) and dashed curves to the model with linear softening and brittleness numbers $\beta = 0.5, 0.2$ and 0.1 . The resulting load-displacement diagrams are shown in Figure 11, first with the inelastic part of elongation on the horizontal axis (Figure 11a), and then with the total elongation on the horizontal axis (Figure 11b). Here, the bar length was set to $L = 10\ell_0$, which is needed to make sure that the localized solution obtained for $\beta = 0.2$ is admissible. For $\beta = 0.1$ (not covered in Figure 11b), a still longer bar would be needed, because the initial size of the damage zone is about $14\ell_0$; see the top curve in Figure 10.

4.3. Model with exponential softening

For concrete and similar quasi-brittle materials, damage laws that lead to a long tail of the softening curve are often used. In the local setting, a suitable shape of the stress-strain diagram is obtained e.g. with the exponential softening law,

$$\sigma = s(\varepsilon) \equiv E\varepsilon_0 \exp\left(-\frac{\varepsilon - \varepsilon_0}{\varepsilon_f}\right), \quad \varepsilon_0 \leq \varepsilon \quad (88)$$

from which

$$g(\varepsilon) = 1 - \frac{s(\varepsilon)}{E\varepsilon} = 1 - \frac{\varepsilon_0}{\varepsilon} \exp\left(-\frac{\varepsilon - \varepsilon_0}{\varepsilon_f}\right), \quad \varepsilon_0 \leq \varepsilon \quad (89)$$

In this case, the relation $\omega = g(\varepsilon)$ cannot be inverted in closed form, but the inverse function g^* can be defined implicitly by the equation

$$(1-\omega)g^*(\omega) \exp\left(\frac{g^*(\omega) - \varepsilon_0}{\varepsilon_f}\right) = \varepsilon_0, \quad 0 \leq \omega \leq 1 \quad (90)$$

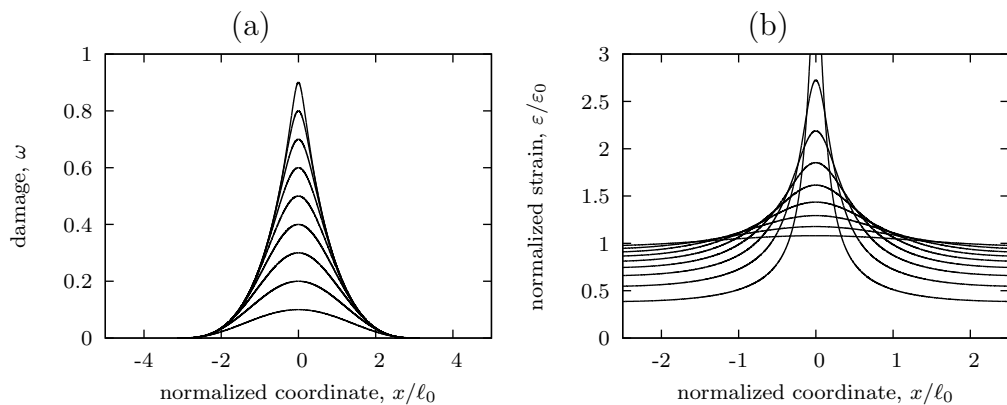


Figure 8: Linear softening: profiles of (a) damage and (b) strain, for $\beta = 0.5$ and ω_{\max} between 0.1 and 0.9.

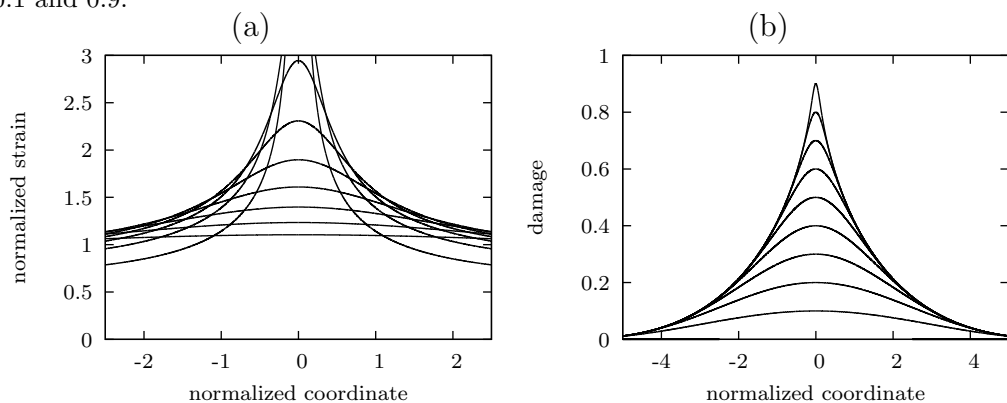


Figure 9: Linear softening: profiles of (a) damage and (b) strain, for $\beta = 0.1$ and ω_{\max} between 0.1 and 0.9.

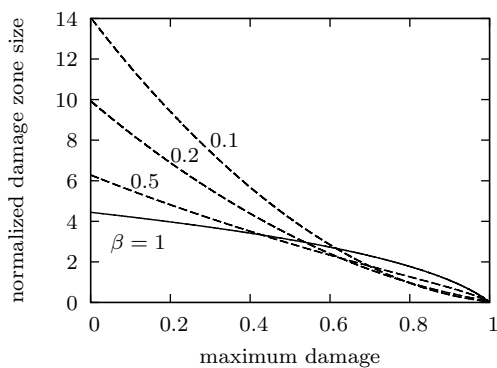


Figure 10: Linear softening: size of the active part of damage zone plotted as a function of maximum damage for different values of brittleness number β .

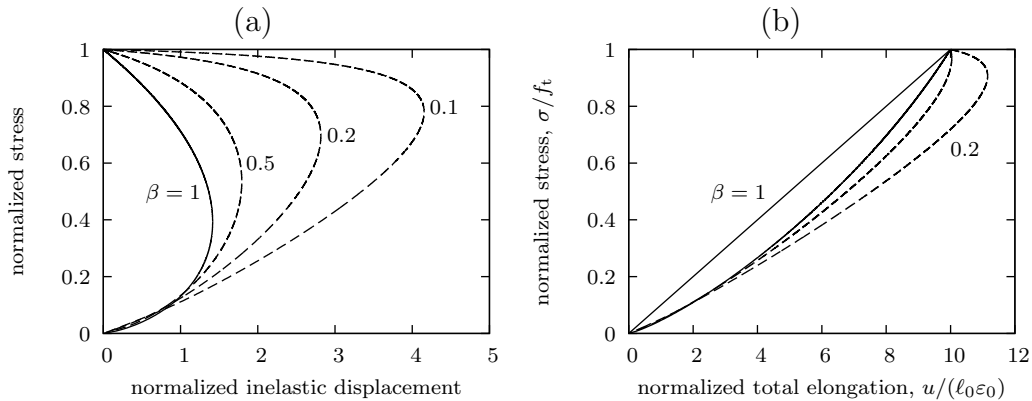


Figure 11: Linear softening: (a) relation between stress and inelastic part of elongation, (b) relation between stress and total elongation (plotted for bar length $L = 10\ell_0$), both for different values of brittleness number β .

The corresponding values of $Y(\omega)$ can then be evaluated by simple substitution into Eq. (72). Note that function D , which would have to be constructed by numerical integration, is not really needed. This function was useful for the formal derivation but it does not appear in the resulting Eq. (76) directly, only through its first derivative Y .

Evolution of the strain and damage profiles is shown in Figure 12 for $\beta = 0.5$ and in Figure 13 for $\beta = 0.1$. Even for exponential softening and a low brittleness number, the active part of the damage zone is shrinking. As seen in Figure 14, the active part of the damage zone approaches a single cross section as the maximum damage tends to 1. This happens for all values of the brittleness number. A low brittleness number β leads to a large initial size of the damage zone but at later stages of the localization process the influence of β fades away.

The load-displacement diagrams in Figure 15 have a similar shape to those corresponding to a model with linear softening. Parameter β affects the initial post-peak slope of the diagram and the amount of dissipated energy, but even for low values of β the diagrams exhibit snapback and eventually return to the origin. Therefore, it seems that an adjustment of the dependence of dissipated energy density on damage is not sufficient to construct a model that exhibits a long tail of the load-displacement diagram. Another modification of the model equations is needed.

5. Modified regularization techniques for elastic-brittle models

5.1. Approach based on gradient of inelastic compliance variable

The results obtained in the previous section indicate that even if the damage law is constructed from a local model with a long tail of the stress-strain diagram,

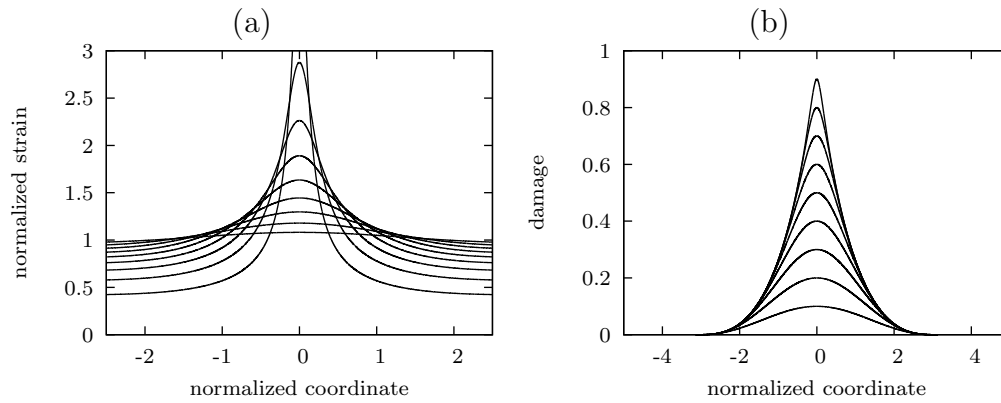


Figure 12: Exponential softening: profiles of (a) strain, (b) damage; all for $\beta = 0.5$.

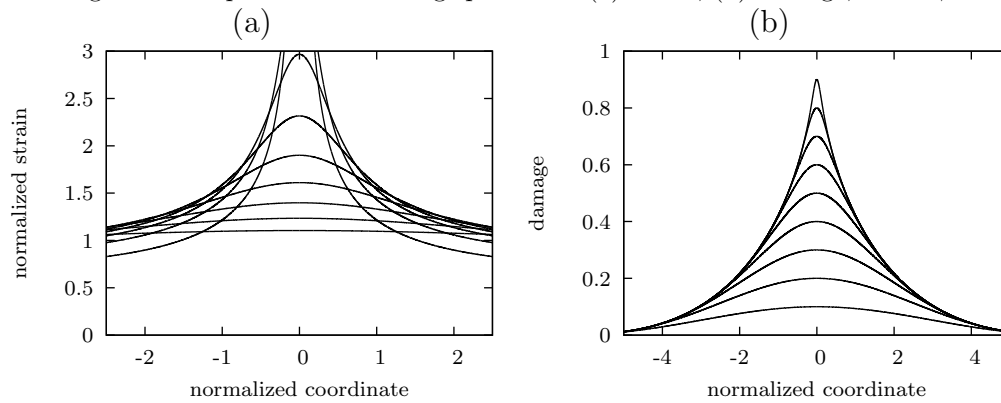


Figure 13: Exponential softening: profiles of (a) strain, (b) damage; all for $\beta = 0.1$.

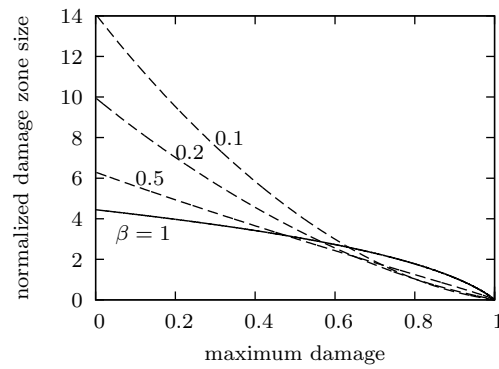


Figure 14: Exponential softening: evolution of the size of damage zone (active part) as a function of maximum damage; solid curve corresponds to elastic-brittle model, dashed curves to exponential softening with $\beta = 0.5$, 0.2 and 0.1 .

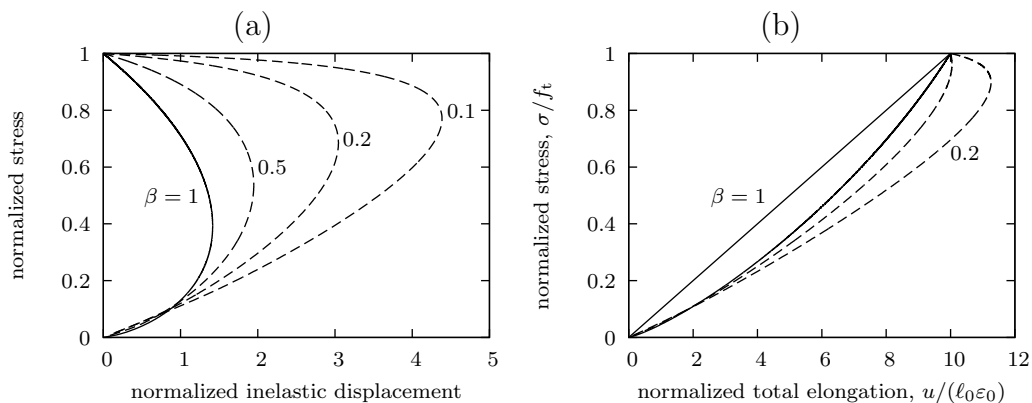


Figure 15: Exponential softening: (a) relation between stress and inelastic part of elongation, (b) relation between stress and total elongation (plotted for bar length $L = 10\ell_0$); solid curve corresponds to elastic-brittle model, dashed curves to exponential softening with different values of brittleness number β .

such as the exponential softening model, the global load-displacement diagram exhibits snapback and the behavior at late stages of the damage process is extremely brittle, which is acceptable only for a certain limited class of materials. Typical load-displacement diagrams of quasi-brittle materials such as concrete possess a long tail. The absence of such a tail in our numerical results is related to the dramatic shrinking of the active part of the damage zone. The primary reason is that the regularizing term based on the damage gradient becomes less powerful at late stages of the process, because the damage variable is bounded by its maximum value 1 and this limit value can be approached at the center of a shrinking damage zone without creating extremely steep damage gradients; see e.g. Figure 13b.

A remedy can be sought in a modification of the regularizing term, based on a transformed variable that approaches infinity as damage approaches 1. A good candidate is the inelastic compliance variable, defined as

$$\gamma = \frac{\omega}{1 - \omega} \quad (91)$$

Its physical meaning can be explained based on the decomposition of strain into the elastic and inelastic parts:

$$\varepsilon = \frac{\sigma}{(1 - \omega)E} = \frac{\sigma}{E} + \left(\frac{1}{1 - \omega} - 1 \right) \frac{\sigma}{E} = \frac{\sigma}{E} + \frac{\omega}{1 - \omega} \frac{\sigma}{E} \quad (92)$$

The first term on the right-hand side is the elastic strain, σ/E , and the second term may be considered as the inelastic part of strain, equal to the elastic strain multiplied by the inelastic compliance variable γ from Eq. (91). During the elastic stage of the response, γ vanishes. As damage evolves and ω approaches 1, γ grows

to infinity, and its gradient can become very steep. Therefore, it can be expected that regularization based on the gradient of γ remains efficient even at late stages of the damage process.

Consider a modified model with $\widehat{\omega}'(x)$ in Eq. (5) replaced by $\widehat{\gamma}'(x)$. The regularizing term is now

$$\mathcal{E}_{\text{reg}}(\widehat{\omega}) = \frac{1}{2} \int_{\Omega} g_{f0} \ell_0^2 \left(\frac{\widehat{\omega}(x)}{1 - \widehat{\omega}(x)} \right)^2 dx = \frac{1}{2} \int_{\Omega} g_{f0} \ell_0^2 \frac{\widehat{\omega}'^2(x)}{(1 - \widehat{\omega}(x))^4} dx \quad (93)$$

The dissipation distance is considered in its generalized form (62), which corresponds to a model with softening. After appropriate modifications, the procedure from Sections 3.1 and 4.1 leads to the governing equation

$$\ell_0^2 \omega''(x) + \frac{2\ell_0^2}{1 - \omega(x)} \omega'^2(x) + \mu(1 - \omega(x))^2 = \frac{(1 - \omega(x))^4}{g_{f0}} Y(\omega(x)) \quad (94)$$

which represents the modified form of Eq. (76).

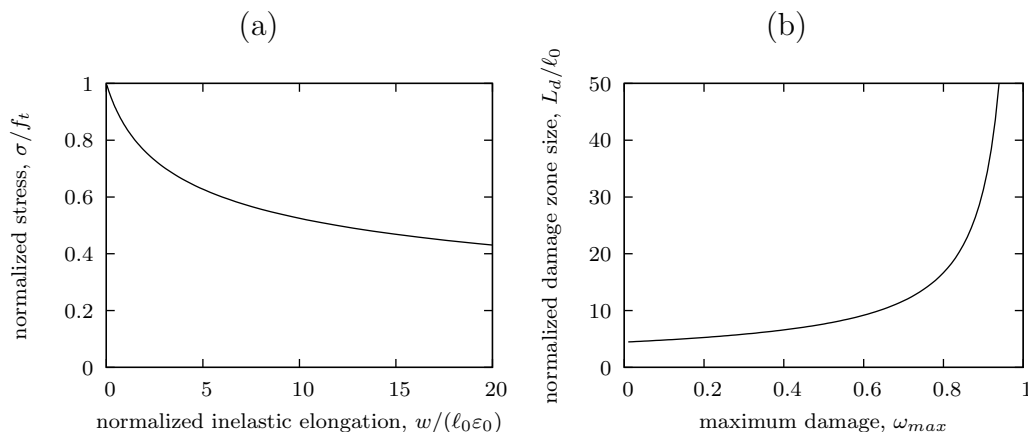


Figure 16: Elastic-brittle model with gradient of inelastic compliance variable: (a) relation between stress and inelastic part of elongation, (b) size of damage zone (active part) as a function of maximum damage.

The numerical solution indeed leads to a long tail of the load-displacement diagram. It is not even necessary to use a model with gradual softening, since the global response is quite ductile already for the locally elastic-brittle model; see Figure 16a. Unfortunately, the ductile response is associated here with an expansion of the damage zone; see Figure 16b and Figure 17a. This is clearly a pathological phenomenon, and the result for a model with linear or exponential softening would be even worse. At late stages, the regularization becomes too strong. If damage is close to 1, small gradients of damage correspond to large gradients of the inelastic compliance variable γ . This is clear from Figure 17b, which shows the evolution of the profile of γ .

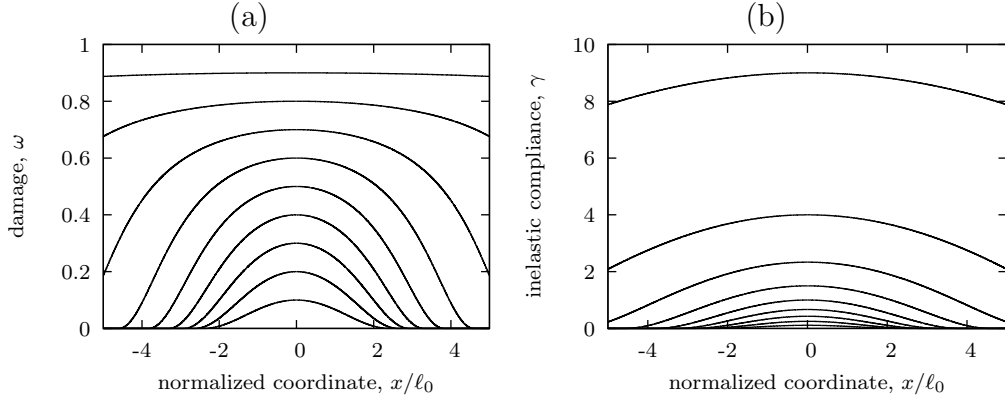


Figure 17: Elastic-brittle model with gradient of inelastic compliance variable: evolution of (a) damage profile, (b) profile of inelastic compliance variable γ .

5.2. Approach based on variable characteristic length

Further modification of the regularizing term can be inspired by an interpretation of Eq. (93) as

$$\mathcal{E}_{\text{reg}}(\widehat{\omega}) = \frac{1}{2} \int_{\Omega} g_{f0} \ell^2(\widehat{\omega}(x)) \widehat{\omega}'^2(x) dx \quad (95)$$

The length parameter ℓ is now considered as variable, dependent on the current damage. For the specific choice

$$\ell(\omega) = \frac{\ell_0}{(1 - \omega)^2} \quad (96)$$

we recover the model from Section 5.2, but it is also possible to use other expressions. The governing equation can be written in the general form

$$\ell^2(\omega(x)) \omega''(x) + \ell(\omega(x)) \ell_{\omega}(\omega(x)) \omega'^2(x) + \frac{\mu}{(1 - \omega(x))^2} = \frac{Y(\omega(x))}{g_{f0}} \quad (97)$$

where $\ell_{\omega} \equiv d\ell/d\omega$. To better control the regularizing effect, we can replace Eq. (96) for instance by

$$\ell(\omega) = \frac{\ell_0}{(1 - \omega)^p} \quad (98)$$

which leads to

$$\ell_{\omega}(\omega) = \frac{d\ell(\omega)}{d\omega} = \frac{p\ell_0}{(1 - \omega)^{p+1}} \quad (99)$$

The exponent p is an adjustable parameter, with $p = 0$ corresponding to the initial formulation based on the gradient of damage (see Section 4) and $p = 2$

to the modified formulation based on the gradient of compliance variable (see Section 5.2).

Let us explore the influence of parameter p on the response of the regularized elastic-brittle model, for which the right-hand side of Eq. (97) is equal to 1. Substituting Eq. (98) and Eq. (99) into Eq. (97) with a unit right-hand side and multiplying both sides by $(1 - \omega)^{2p+1}$, we obtain the nonlinear second-order differential equation

$$(1 - \omega(x))\ell_0^2\omega''(x) + p\ell_0^2\omega'^2(x) + (1 - \omega(x))^{2p-1}\mu = (1 - \omega(x))^{2p+1} \quad (100)$$

At the onset of damage, we have $\omega_1(x) = 0$ and $\mu = 1$, and the initial damage rate $\dot{\omega}_1(x)$ is governed by the same linear second-order differential equation (40) as in Section 3.3. The localized solutions satisfying the boundary conditions have again the form given by (44), i.e.,

$$\dot{\omega}_1(x) = -\frac{\dot{\mu}_1}{2} \left(1 + \cos \frac{\sqrt{2}x}{\ell_0} \right), \quad -\frac{\pi\ell_0}{\sqrt{2}} \leq x \leq \frac{\pi\ell_0}{\sqrt{2}} \quad (101)$$

provided that the center of the localized damage zone is at the origin.

Eq. (101) describes the initial damage rate, just after localization. Now we search for possible solutions that preserve the size of the damage zone and the shape of the damage profile even after a finite increment. The assumed form of the solution is thus

$$\omega(x) = A(\mu) \left(1 + \cos \frac{\sqrt{2}x}{\ell_0} \right), \quad -\frac{L_d}{2} \leq x \leq \frac{L_d}{2} \quad (102)$$

where $L_d = \sqrt{2}\pi\ell_0$ and $A(\mu)$ is a yet unknown function of the loading parameter μ . Substituting (102) into Eq. (100), we find that the assumed type of solution exists if $p = 0.5$, and then $A(\mu) = (1 - \mu)/2$. Since $\omega(0) = 2A(\mu)$ is the maximum value of damage at the center of the damage zone, ω_{\max} , we get a linear relation between the load parameter μ and the maximum damage. Recall that, for the elastic-brittle model, $\mu = \sigma^2/f_t^2$ where f_t is the tensile strength. Consequently, $\sigma = f_t\sqrt{1 - \omega_{\max}}$.

It is also possible to derive an analytical expression for the inelastic part of elongation corresponding to a given stress level, similar to (60):

$$\begin{aligned} w &= \frac{\sigma}{E} \left(\int_{-L_d/2}^{L_d/2} \frac{dx}{1 - \omega(x)} - L_d \right) = \\ &= \frac{\sigma}{E} \left(\int_{-\pi\ell_0/\sqrt{2}}^{\pi\ell_0/\sqrt{2}} \frac{2 dx}{1 + \mu - (1 - \mu) \cos \frac{\sqrt{2}x}{\ell_0}} - L_d \right) = \end{aligned}$$

$$= \frac{\sigma}{E} \left(\frac{2\ell_0}{\sqrt{2\mu}} \left[\arctan \frac{\tan \frac{x}{\sqrt{2\ell_0}}}{\sqrt{\mu}} \right]_{-\pi\ell_0/\sqrt{2}}^{\pi\ell_0/\sqrt{2}} - L_d \right) = \frac{\sigma}{E} \left(\frac{\sqrt{2\pi\ell_0}}{\sqrt{\mu}} - L_d \right) \quad (103)$$

Taking into account that $\mu = \sigma^2/f_t^2$ and $L_d = \sqrt{2\pi\ell_0}$, we finally get

$$w = \frac{\sigma}{E} \left(\frac{\sqrt{2\pi\ell_0}f_t}{\sigma} - \sqrt{2\pi\ell_0} \right) = \frac{\sqrt{2\pi\ell_0}}{E} (f_t - \sigma) \quad (104)$$

This means that the softening part of the load-displacement diagram is in this case linear and the final elongation at complete failure is

$$w_f = \frac{\sqrt{2\pi\ell_0}f_t}{E} = \sqrt{2\pi\ell_0}\varepsilon_0 = L_d\varepsilon_0 \quad (105)$$

Of course, the load-displacement diagram exhibits snapback, because the elongation at peak load is $L\varepsilon_0$ where L is the total length of the bar, while the final elongation is $L_d\varepsilon_0$, where $L_d = \sqrt{2\pi\ell_0}$ is the size of the localized damage zone, which must be smaller than the bar length, otherwise the localized solution considered here would not be valid. Nevertheless, the model is regularized because the total energy dissipated by failure is nonzero and equals $L_d\varepsilon_0 A f_t/2$. The energy dissipated per unit sectional area is thus $G_f = L_d\varepsilon_0 f_t/2 = L_d g_{f0}$. It corresponds to the energy dissipated per unit volume, g_{f0} , multiplied by the size of the damage zone, L_d , which is proportional to the internal length parameter ℓ_0 .

The results of our analysis are confirmed by numerical simulations. Figure 18a shows the size of the active part of damage zone as a function of the maximum damage. Note that the top and bottom plots differ only by the scale on the vertical axis. The horizontal solid line corresponds to $p = 0.5$, for which the damage zone remains constant and its size is $\sqrt{2\pi\ell_0}$, as expected. For comparison, curves that correspond to selected values of p different from 0.5 are plotted as well. For $p = 0.4$, the active part of the damage zone gradually shrinks to a single cross section. For $p = 0.6$, the damage zone expands, but only slightly. The expansion is more pronounced for higher values of p . Figure 18b shows the inelastic part of the stress-displacement diagram, again for different values of exponent p . It is confirmed that the global softening diagram is linear for $p = 0.5$. For lower values of exponent p , the diagram snaps back to the origin, and for higher values it exhibits a tail, which is very long for $p = 1$ or 2; see the bottom plot in Figure 18b.

The evolution of damage and strain profiles for $p = 0.4, 0.5, 0.6$ and 1.0 (from top to bottom) is plotted in Figure 19. The profiles correspond to values of maximum damage ranging from 0.1 to 0.9 with step 0.1, and the last profile corresponds to $\omega_{\max} = 0.9999$. The damage zone shrinks for $p < 0.5$ and expands for $p > 0.5$, see Figure 19a, while the strain profile gets more concentrated not only for $p < 0.5$

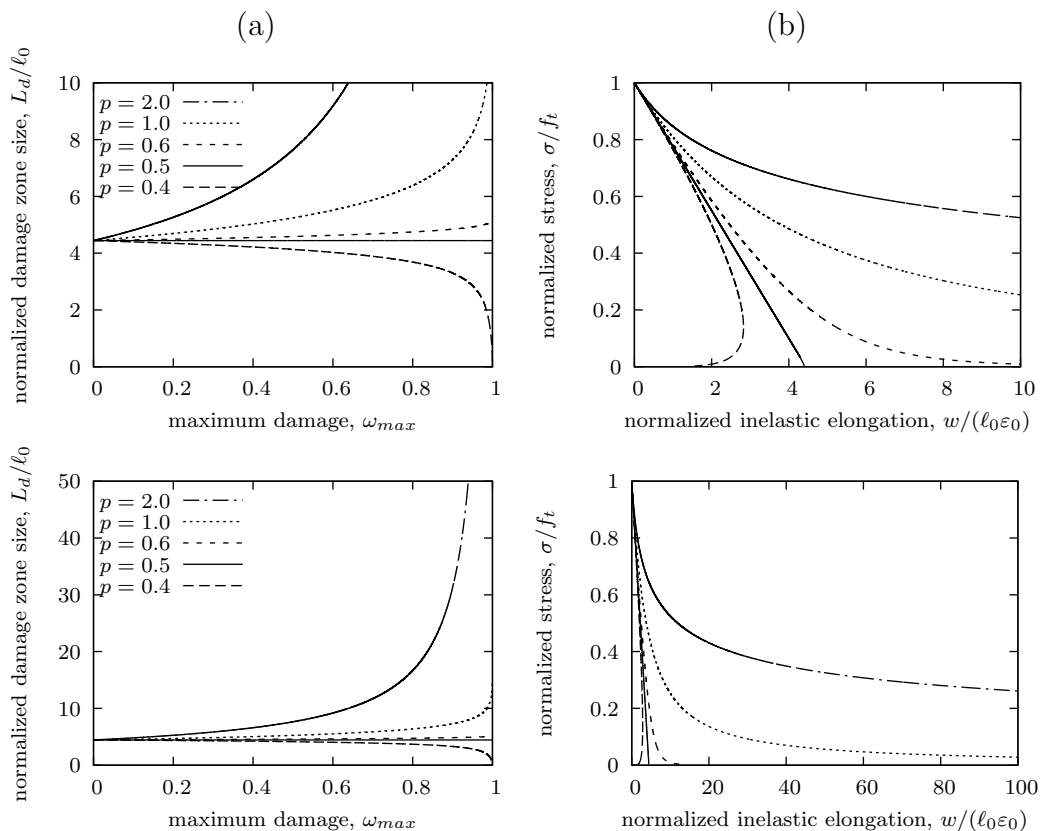


Figure 18: Regularized elastic-brittle model with variable characteristic length given by Eq. (98) and with different values of exponent p : (a) size of damage zone (active part) as a function of maximum damage, (b) relation between stress and inelastic part of elongation.

but also for somewhat higher values, e.g. for $p = 0.6$ (but not for $p = 1$), see Figure 19b. The shapes of the “final” profiles of strain and damage at $\omega_{max} = 0.9999$ are compared in Figure 20, with $p = 0.8$ included in the comparison.

5.3. Alternative interpretation – approach based on generalized compliance variable

Recall that the modified model with variable characteristic length given by Eq. (98) has been motivated by the special case with $p = 2$, which is equivalent to a model with constant characteristic length and gradient of the inelastic compliance variable γ defined in Eq. (91). Even for values of p different from 2, the regularizing term can be written in the form

$$\mathcal{E}_{reg} = \frac{1}{2} \int_{\Omega} g_{f0} \ell_0^2 \gamma'^2(x) dx \quad (106)$$

however, with a generalized definition of the inelastic compliance variable. The appropriate expression for γ in terms of ω can be constructed from the condition

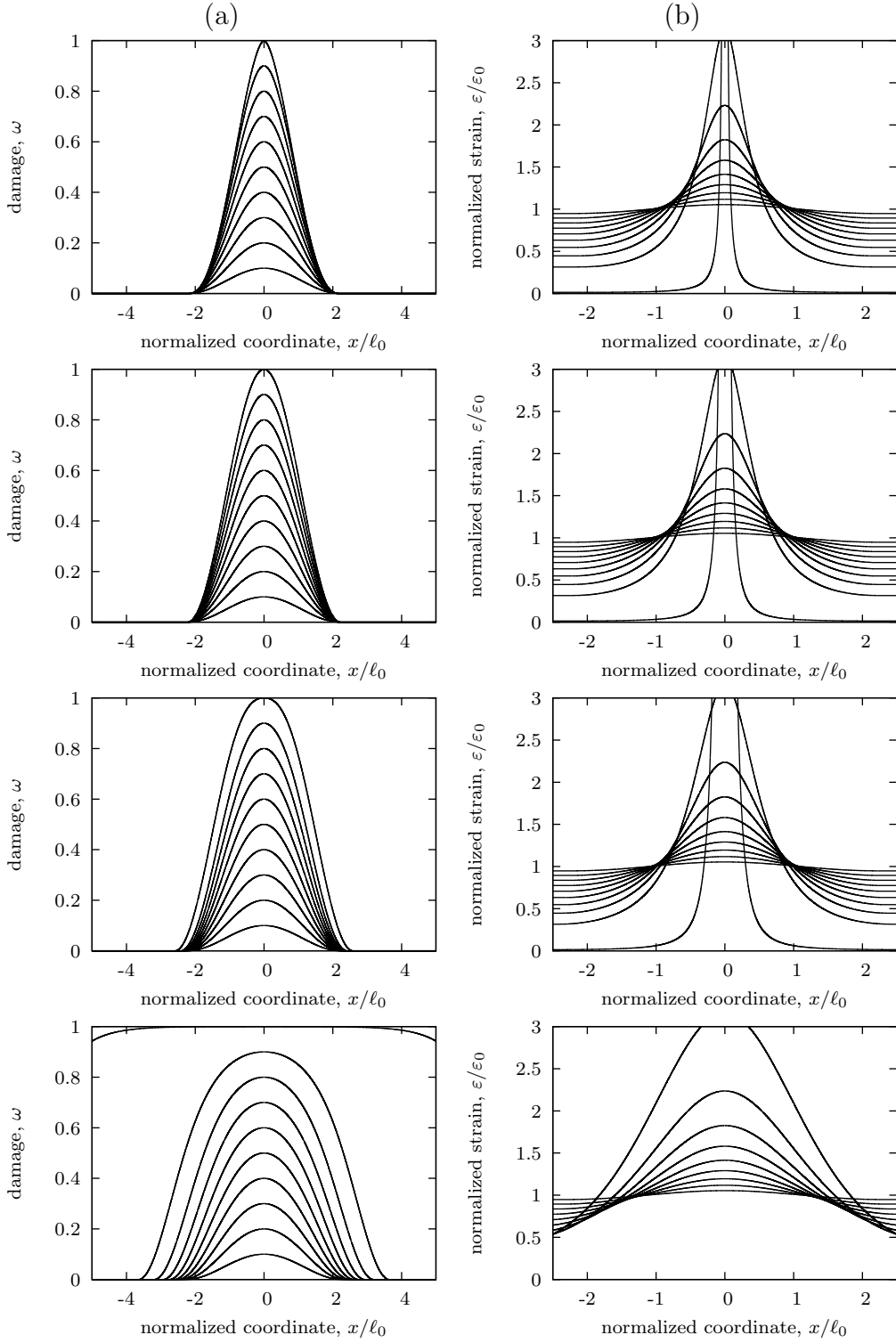


Figure 19: Regularized elastic-brittle model with variable characteristic length given by Eq. (98) and different values of exponent $p = 0.4, 0.5, 0.6$ and 1.0 (from top to bottom): evolution of (a) damage profile, (b) strain profile.

$\ell_0 \gamma' = \ell(\omega) \omega'$. This condition can be rewritten as

$$\ell_0 \frac{d\gamma}{d\omega} = \ell(\omega) \quad (107)$$

from which

$$\gamma(\omega) - \gamma(0) = \frac{1}{\ell_0} \int_0^\omega \ell(\tilde{\omega}) d\tilde{\omega} \quad (108)$$

For the specific dependence of characteristic length on damage given by Eq. (98), evaluation of the integral and application of the condition $\gamma(0) = 0$ leads to

$$\gamma(\omega) = \int_0^\omega \frac{d\tilde{\omega}}{(1-\tilde{\omega})^p} = \begin{cases} \frac{1 - (1-\omega)^{1-p}}{1-p} & \text{for } p \neq 1 \\ \ln \frac{1}{1-\omega} & \text{for } p = 1 \end{cases} \quad (109)$$

Indeed, for $p = 2$ this reduces to the standard definition of inelastic compliance variable (91) and for $p = 0$ to $\gamma(\omega) = \omega$. The special case of $p = 0.5$ gives

$$\gamma(\omega) = 2(1 - \sqrt{1-\omega}) \quad (110)$$

So the model that leads to a stationary size of damage zone can be considered as a model with regularizing term in the form of Eq. (106) in which the inelastic compliance variable is given by Eq. (110). The evolution of the profiles of this inelastic compliance variable is shown in Figure 21.

6. Modified regularization techniques for models with softening

In Section 4 it was shown that incorporation of softening (gradual damage growth) in combination with the simplest regularization approach based on gradient of damage and constant characteristic length is not sufficient to produce global load-displacement diagrams with a tail, even if the softening law is constructed such that the local response (in the absence of localization) is very ductile. Therefore, it is interesting to examine the combination of softening models with the modified regularization techniques developed in Section 5 for the elastic-brittle model. This combination provides the most general and most flexible framework, which covers the models from all the previous sections as special cases.

A fully general formulation is obtained if the regularizing part of stored energy is defined by formula (95) and the dissipation distance by formula (62). For convenience, both expressions are reproduced here:

$$\mathcal{E}_{\text{reg}}(\hat{\omega}) = \frac{1}{2} \int_{\Omega} g_{f0} \ell^2(\hat{\omega}(x)) \hat{\omega}'^2(x) dx \quad (111)$$

$$\mathcal{D}(\hat{\omega}_1, \hat{\omega}_2) = \begin{cases} \int_{\Omega} (D(\hat{\omega}_2(x)) - D(\hat{\omega}_1(x))) dx & \text{if } \hat{\omega}_2 \geq \hat{\omega}_1 \text{ in } \Omega \\ +\infty & \text{otherwise} \end{cases} \quad (112)$$

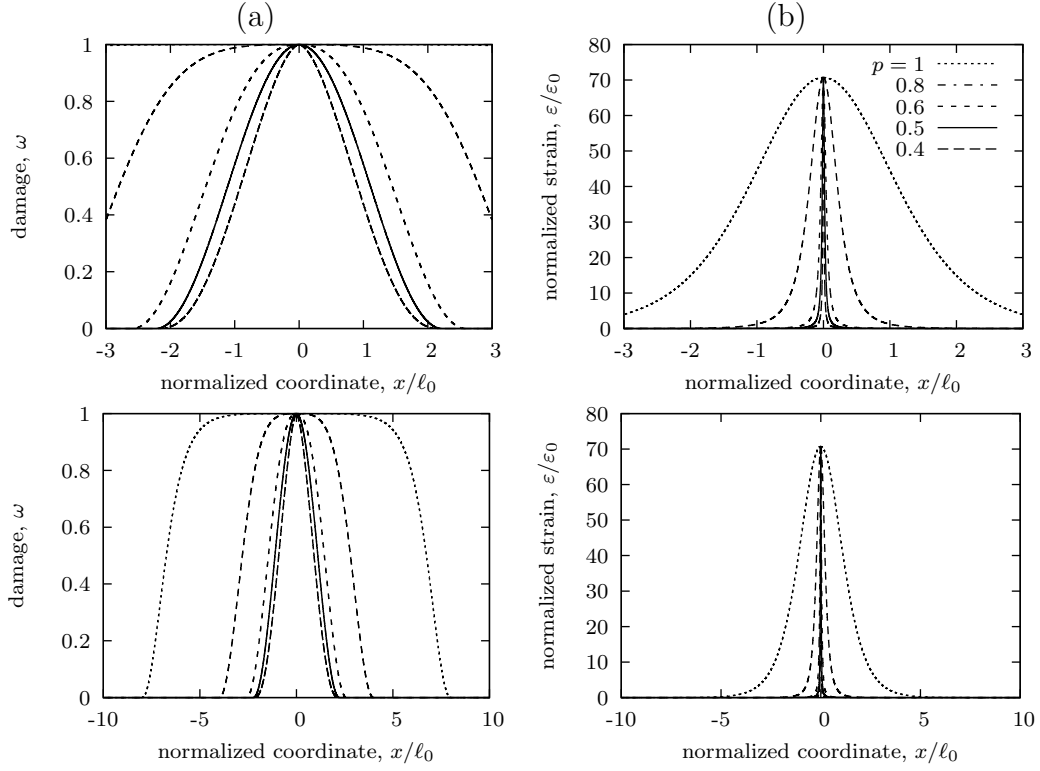


Figure 20: Regularized elastic-brittle model with variable characteristic length given by Eq. (98): comparison of (a) damage profiles and (b) strain profiles at $\omega_{\max} = 0.9999$ for different values of exponent $p = 1, 0.8, 0.6, 0.5$ and 0.4 .

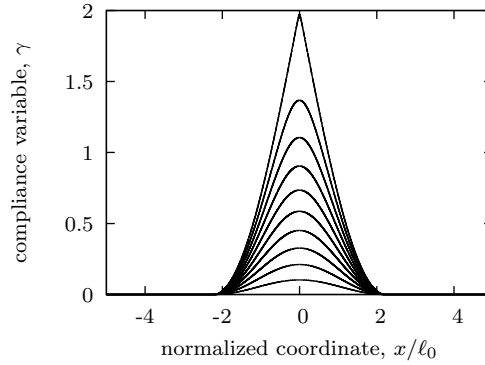


Figure 21: Regularized elastic-brittle model with variable characteristic length given by Eq. (98) with $p = 0.5$: profiles of generalized inelastic compliance variable γ defined by Eq. (110).

Recall that ℓ in Eq. (111) is the damage-dependent characteristic length, which can be defined e.g. by formula (98), and D in (112) is the dissipation density function, the derivative of which is the damage energy release rate Y . For the model with linear softening, the dependence of Y on damage is given explicitly by Eq. (84), while for exponential softening it is described implicitly by equations (72) and (90). If ℓ is set to a constant, ℓ_0 , the formulation reduces to the simple regularization technique based on the damage gradient, treated in Sections 2–4. If Y is set to a constant, g_{f0} , the underlying damage model reduces to the elastic-brittle model, treated in Sections 2, 3, and 5.

The differential equation that needs to be satisfied in the damage zone has in fact already been presented in Section 5.2 as Eq. (97). The analysis in Section 5.2 has been performed for the elastic-brittle case only, with the right-hand side of Eq. (97) set to 1. Now we can explore the cases when Y corresponds to linear or exponential softening, as explained in the previous paragraph. For linear softening with different values of brittleness β defined in Eq. (80), the dependence of the damage zone size on maximum damage and the inelastic part of the stress-elongation diagram are shown in Figure 22. For $\beta = 1$, the results are plotted by the solid curves and correspond to the elastic-brittle model from Section 3.

The results are also affected by exponent p in formula (98) for the characteristic length. Let us first look at the case of $p = 0.5$, for which the elastic-brittle model gives a constant size of the damage zone and a linear post-peak part of the stress-elongation diagram. Numerical results plotted in Figure 22 indicate that with decreasing β (i.e., with increasing ductility of the underlying local model), the initial size of the damage zone increases and the magnitude of the initial post-peak slope decreases, but the final inelastic displacement at complete failure remains the same, independent of β . This is related to pronounced shrinking of the active part of damage zone during the localization process. For lower values of β it shrinks from a higher initial value to a lower final value, which results into an increased slope of the stress-elongation diagram and even into snapback.

Interestingly, the behavior of the model with exponential softening and $p = 0.5$ is very similar; see Figure 23. The final value of inelastic elongation remains independent of the brittleness number and no tail of the stress-elongation diagram can be produced, even if the local damage law corresponds to a very ductile behavior (i.e., if β is very small).

Based on the results obtained for the elastic-brittle case, we can expect that a tail should appear for values of exponent p higher than 0.5, but at the same time there is a danger that the damage zone would expand.

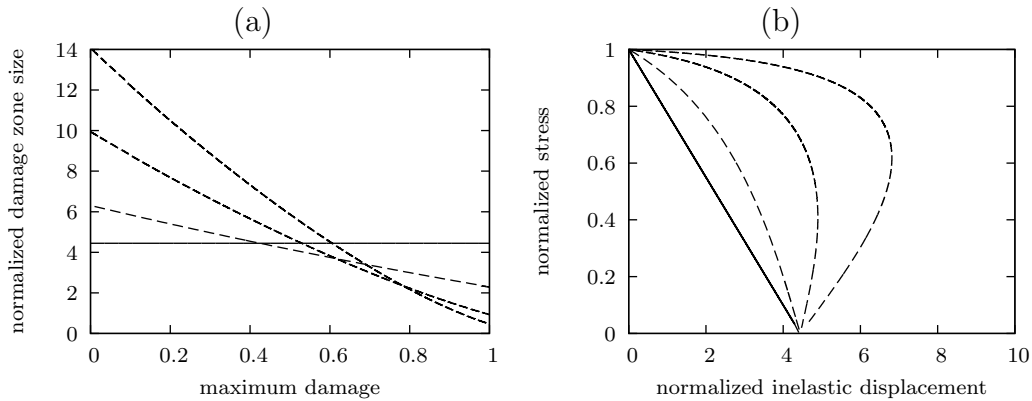


Figure 22: Regularized **linear softening** model with variable characteristic length given by Eq. (98), with exponent $p = 0.5$ and different values of brittleness $\beta = 1, 0.5, 0.2$ and 0.1 : (a) size of damage zone (active part) as a function of maximum damage, (b) relation between stress and inelastic part of elongation.

7. Summary and conclusions

Several versions of regularized damage models based on a variational approach have been described and their localization properties have been examined. All of these models construct the functions describing the displacement field and the damage field by incremental minimization of a certain energetic functional. Individual models differ by the specific definitions of stored energy and dissipation distance, which are needed to construct the corresponding energetic functional. Optimality conditions lead to a consistent set of equations and inequalities which characterize the displacements and damage in the elastic zone, damage zone, at their interface and at the physical boundary of the body.

The point of departure was the regularized elastic brittle model with stored energy consisting of the standard part (4) and regularizing part (5) and with dissipation distance (6). Its localization properties under uniaxial stress were examined in Section 3 based on (i) linear differential equation (38) which characterizes the initial damage rate at bifurcation from a uniform state, and (ii) nonlinear differential equation (31) which characterizes the damage profile after a generic incremental step. The linear rate equation was shown to have an analytical solution while the nonlinear equation was solved by an incremental-iterative procedure. It was found that the active part of the damage zone contracts down to zero size during the failure process, and that the dissipated energy is finite but the load-displacement (or stress-elongation) diagram is quite brittle and exhibits snapback even for short bars (with respect to the characteristic length of the material). This kind of model would be suitable for brittle materials but not for quasi-brittle ones, which typically exhibit a long tail of the load-displacement diagram.

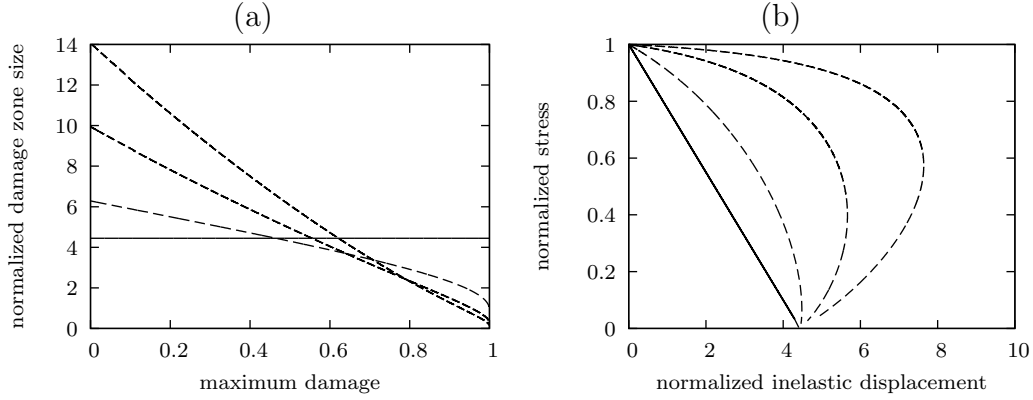


Figure 23: Regularized **exponential softening** model with variable characteristic length given by Eq. (98), with exponent $p = 0.5$ and different values of brittleness $\beta = 1, 0.5, 0.2$ and 0.1 : (a) size of damage zone (active part) as a function of maximum damage, (b) relation between stress and inelastic part of elongation.

To provide more flexibility and to better control the inelastic part of the load-displacement diagram, modified versions of the model were proposed and examined. First of all, softening in the sense of gradual decrease of stress under uniform conditions was added in Section 4 by generalizing the dissipation distance; see formulae (62) and (73). However, numerical simulations revealed that the enhanced ductility of the material affects only the initial size of the damage zone and the initial post-peak slope of the load-displacement diagram. At later stages of the failure process, the damage zone contracts again to zero size and the load-displacement diagram exhibits snapback and returns to the origin. This happens even for a model constructed such that its stress-strain diagram under uniform strain would have an exponential tail.

As an alternative, a modification of the regularizing part of the stored energy was proposed in Section 5. In its simplest form (93), it replaces the damage gradient by the gradient of the inelastic compliance variable (91), which represents a transformed characteristic of damage that tends to infinity as complete failure is approached (unlike damage, which tends to 1). This simple modification was found to revert the contraction of the damage zone into its expansion and to produce an extremely ductile response with stress locking effects. Therefore, a more general definition of compliance variable (109) was devised, with parameter p allowing to tune up the model behavior. As special cases, the original model with regularizing term (5) is recovered for $p = 0$ and the simplest form of modified model with regularizing term (93) is recovered for $p = 2$. It was found that the size of the damage zone remains constant for $p = 0.5$, increases for $p > 0.5$ and decreases for $p < 0.5$. Expansion of the damage zone leads to longer tails of the load-displacement diagram. It was also demonstrated that the formulation with

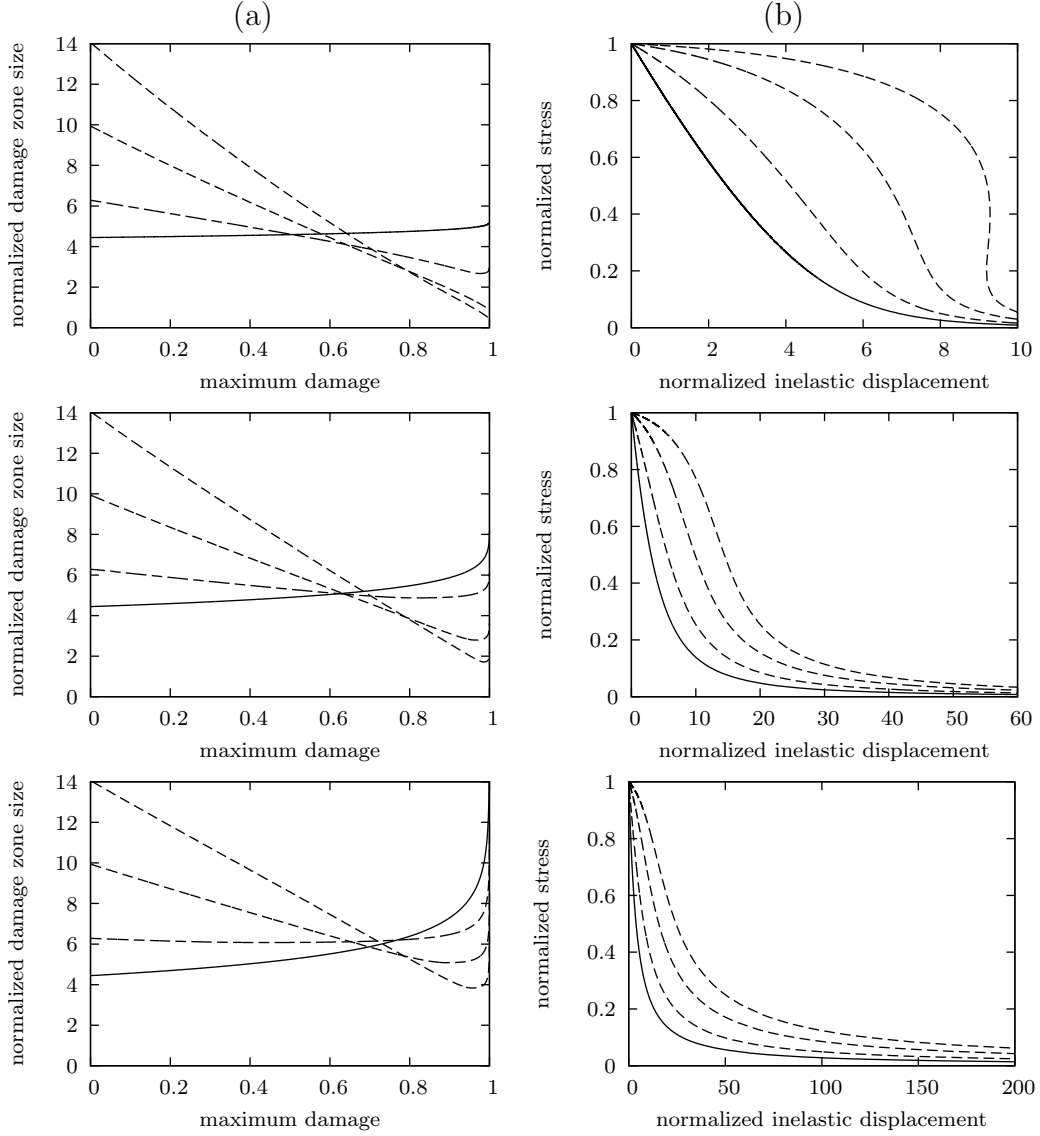


Figure 24: Regularized **exponential softening** model with variable characteristic length given by Eq. (98), with exponents $p = 0.6, 0.8$ and 1.0 (from top to bottom) and different values of brittleness $\beta = 1, 0.5, 0.2$ and 0.1 : (a) size of damage zone (active part) as a function of maximum damage, (b) relation between stress and inelastic part of elongation.

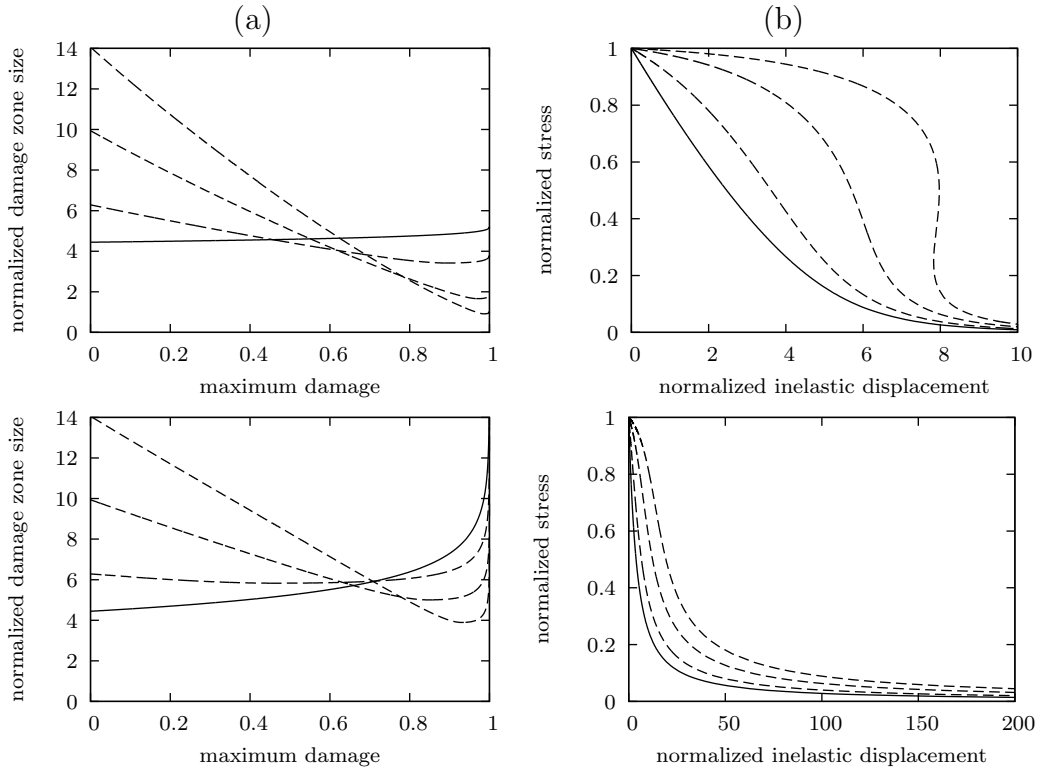


Figure 25: Regularized **linear softening** model with variable characteristic length given by Eq. (98), with exponents $p = 0.6$ and 1.0 (from top to bottom) and different values of brittleness $\beta = 1, 0.5, 0.2$ and 0.1 : (a) size of damage zone (active part) as a function of maximum damage, (b) relation between stress and inelastic part of elongation.

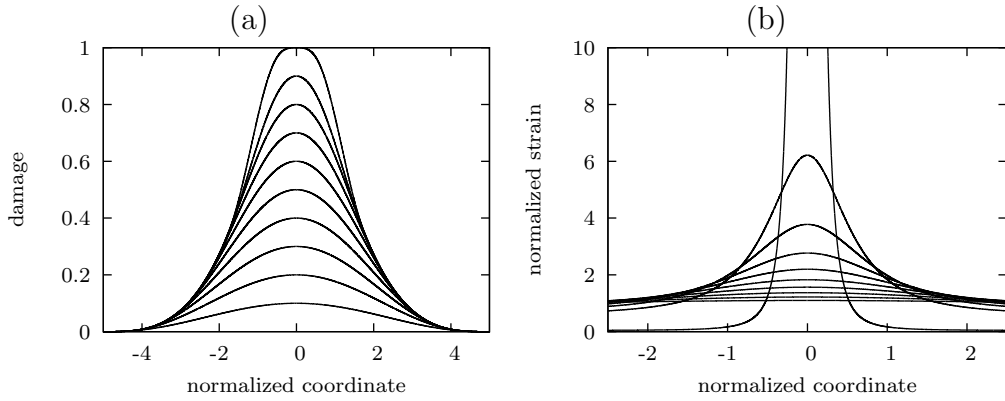


Figure 26: Regularized **exponential softening** model with variable characteristic length given by Eq. (98) and exponent $p = 0.8$ and brittleness $\beta = 0.2$: evolution of (a) damage profile, (b) strain profile.

the gradient of generalized compliance variable is fully equivalent to a formulation with the gradient of damage combined with a variable characteristic length; see (95).

Finally, a combination of softening incorporated through the dissipation distance with the modified regularization based on variable characteristic length was examined in Section 6. It was shown that realistic shapes of the load-displacement diagram can be obtained for certain combinations of parameter p and another parameter β that describes the ductility under uniform conditions.

To keep the present study focused, its scope has been limited to localization analysis in the one-dimensional setting, with physical interpretation in terms of a bar under uniaxial tension. Alternatively, the same governing equations with a different meaning of individual symbols could describe an infinite shear layer. Such a simplified analysis has revealed some of the basic features of the initial model and of its numerous modifications and indicated which general trends could be expected in a more general setting (e.g., expansion or contraction of the damage zone, and brittle or ductile character of the load-displacement diagram). Of course, certain other aspects cannot be investigated in 1D and would need to be addressed by at least two-dimensional analytical studies and numerical simulations.

As pointed out by Simone et al. (2004), simulations of notched specimens based on integral-type nonlocal damage models exhibit certain pathological or at least questionable features. For instance, damage is initiated not directly at the tip of a notch or pre-existing crack but at a finite distance from the tip, proportional to the characteristic length of the nonlocal model. The reason is that integral-type nonlocal models usually consider damage as driven by nonlocal equivalent strain, obtained by weighted spatial averaging of locally evaluated equivalent strains. The local strain has a singularity at the crack tip but the nonlocal strain remains bounded and turns out to have a maximum at a certain distance from the tip. It is worth noting that for sufficiently low load levels the maximum nonlocal strain remains below the damage threshold and the response remains purely elastic, with a stress singularity. In contrast to that, the present gradient-based damage model can be expected to initiate damage right at the crack tip and for arbitrarily low load levels, because the singular strain field corresponding to linear elastic fracture mechanics would immediately violate the multi-dimensional version of condition (21), with the second derivative of damage replaced by the Laplacean of damage and with the term $\frac{1}{2}Eu_k'^2$ replaced by the proper expression for elastic energy density under multiaxial stress.

The issue of damage initiation at or near a notch tip is closely related to the subsequent evolution of the damage zone and of stresses within this zone, and to the final distribution of dissipated energy in the vicinity of the notch. As shown in detailed studies of such phenomena (Jirásek et al., 2004; Grassl et al., 2014),

integral-type nonlocal damage models with standard normalization of the nonlocal weight function near boundaries lead to excessive values of stresses and dissipation density in the vicinity of a notch. Such spurious phenomena can be to a large extent reduced by special modifications, e.g. by a reduction of the characteristic length near boundaries. Whether the present gradient-based formulation has a similar effect needs to be assessed by numerical simulations, which are left for further research.

Acknowledgments

The authors would like to acknowledge the financial support from the Czech Science Foundation (project No. 108/11/1243). They would also like to thank the reviewers for careful reading of the manuscript and for helpful and stimulating comments.

References

- Bažant, Z.P., 1976. Instability, ductility, and size effect in strain-softening concrete. *Journal of the Engineering Mechanics Division* 102, 331–344.
- Bažant, Z.P., Jirásek, M., 2002. Nonlocal integral formulations of plasticity and damage: Survey of progress. *Journal of Engineering Mechanics* 128, 1119–1149. doi:[10.1061/\(ASCE\)0733-9399\(2002\)128:11\(1119\)](https://doi.org/10.1061/(ASCE)0733-9399(2002)128:11(1119)).
- Bouchitté, G., Mielke, A., Roubíček, T., 2009. A complete-damage problem at small strains. *Zeitschrift für Angewandte Mathematik und Physik* 60, 205–236. doi:[10.1007/s00033-007-7064-0](https://doi.org/10.1007/s00033-007-7064-0).
- Braides, A., 2014. Local Minimization, Variational Evolution and Γ -Convergence. Number 2094 in *Lecture Notes in Mathematics*, Springer, New York. doi:[10.1007/978-3-319-01982-6](https://doi.org/10.1007/978-3-319-01982-6).
- Di Luzio, G., Bažant, Z.P., 2005. Spectral analysis of localization in nonlocal and over-nonlocal materials with softening plasticity or damage. *International Journal of Solids and Structures* 42, 6071–6100. doi:[10.1016/j.ijsolstr.2005.03.038](https://doi.org/10.1016/j.ijsolstr.2005.03.038).
- Engelen, R.A.B., Fleck, N.A., Peerlings, R.H.J., Geers, M.G.D., 2006. An evaluation of higher-order plasticity theories for predicting size effects and localisation. *International Journal of Solids and Structures* 43, 1857–1877. doi:[10.1016/j.ijsolstr.2004.05.072](https://doi.org/10.1016/j.ijsolstr.2004.05.072).
- Frémond, M., Nedjar, B., 1996. Damage, gradient of damage and principle of virtual power. *International Journal of Solids and Structures* 33, 1083–1103. doi:[10.1016/0020-7683\(95\)00074-7](https://doi.org/10.1016/0020-7683(95)00074-7).

- Friedman, A., 1982. Variational Principles and Free-Boundary Problems. Wiley, New York.
- Grassl, P., Xenos, D., Jirásek, M., Horák, M., 2014. Evaluation of nonlocal approaches for modelling fracture near nonconvex boundaries. *International Journal of Solids and Structures* 51, 3239–3251. doi:[10.1016/j.ijsolstr.2014.05.023](https://doi.org/10.1016/j.ijsolstr.2014.05.023), [arXiv:1406.3381](https://arxiv.org/abs/1406.3381).
- Jahn, J., 2007. Introduction to the Theory of Nonlinear Optimization. third ed., Springer.
- Jirásek, M., 1998. Nonlocal models for damage and fracture: Comparison of approaches. *International Journal of Solids and Structures* 35, 4133–4145. doi:[10.1016/S0020-7683\(97\)00306-5](https://doi.org/10.1016/S0020-7683(97)00306-5).
- Jirásek, M., Bažant, Z., 2002. Inelastic Analysis of Structures. John Wiley & Sons, Chichester, England.
- Jirásek, M., Rokoš, O., Zeman, J., 2013. Localization analysis of variationally based gradient plasticity model. *International Journal of Solids and Structures* 50, 256–269. doi:<http://dx.doi.org/10.1016/j.ijsolstr.2012.09.022>, [arXiv:1102.5271](https://arxiv.org/abs/1102.5271).
- Jirásek, M., Rolshoven, S., 2003. Comparison of integral-type nonlocal plasticity models for strain-softening materials. *International Journal of Engineering Science* 41, 1553–1602. doi:[10.1016/S0020-7225\(03\)00027-2](https://doi.org/10.1016/S0020-7225(03)00027-2).
- Jirásek, M., Rolshoven, S., 2009a. Localization properties of strain-softening gradient plasticity models. Part I: Strain gradient theories. *International Journal of Solids and Structures* 46, 2225–2238. doi:[10.1016/j.ijsolstr.2008.12.016](https://doi.org/10.1016/j.ijsolstr.2008.12.016).
- Jirásek, M., Rolshoven, S., 2009b. Localization properties of strain-softening gradient plasticity models. Part II: Theories with gradients of internal variables. *International Journal of Solids and Structures* 46, 2239–2254. doi:[10.1016/j.ijsolstr.2008.12.018](https://doi.org/10.1016/j.ijsolstr.2008.12.018).
- Jirásek, M., Rolshoven, S., Grassl, P., 2004. Size effect on fracture energy induced by non-locality. *International Journal for Numerical and Analytical Methods in Geomechanics* 28, 653–670. doi:[10.1002/nag.364](https://doi.org/10.1002/nag.364).
- Kachanov, L.M., 1958. Time of the rupture process under creep conditions. *Izvestia Akademii Nauk SSSR, Otdelenie Tekhnicheskikh Nauk* 8, 26–31. doi:[10.1023/A:1018671022008](https://doi.org/10.1023/A:1018671022008).

- Mielke, A., 2005. Evolution of rate-independent systems, in: Dafermos, C., Feireisl, E. (Eds.), *Handbook of Differential Equations: Evolutionary Equations*. Elsevier B.V., Amsterdam, The Netherlands. volume 2, pp. 461–559.
- Mielke, A., 2011a. Complete-damage evolution based on energies and stresses. *Discrete and Continuous Dynamical Systems - Series S* 4, 423–439. doi:[10.3934/dcdss.2011.4.423](https://doi.org/10.3934/dcdss.2011.4.423).
- Mielke, A., 2011b. Differential, energetic, and metric formulations for rate-independent processes, in: Ambrosio, L., Savaré, G. (Eds.), *Nonlinear PDE's and Applications*. Springer, Berlin, Heidelberg. number 2011 in *Lecture Notes in Mathematics*, pp. 87–170.
- Mielke, A., Roubíček, T., 2006. Rate-independent damage processes in nonlinear elasticity. *Mathematical Models and Methods in Applied Sciences* 16, 177–209. doi:[10.1142/S021820250600111X](https://doi.org/10.1142/S021820250600111X).
- Mielke, A., Roubíček, T., Zeman, J., 2010. Complete damage in elastic and viscoelastic media and its energetics. *Computer Methods in Applied Mechanics and Engineering* 199, 1242–1253. doi:[10.1016/j.cma.2009.09.020](https://doi.org/10.1016/j.cma.2009.09.020).
- Peerlings, R.H.J., Geers, M.G.D., de Borst, R., Brekelmans, W.A.M., 2001. A critical comparison of nonlocal and gradient-enhanced softening continua. *International Journal of Solids and Structures* 38, 7723–7746. doi:[10.1016/S0020-7683\(01\)00087-7](https://doi.org/10.1016/S0020-7683(01)00087-7).
- Pham, K., Marigo, J.J., 2010a. The variational approach to damage: I. The foundations. *Comptes Rendus Mécanique* 338, 191–198. doi:[10.1016/j.crme.2010.03.009](https://doi.org/10.1016/j.crme.2010.03.009).
- Pham, K., Marigo, J.J., 2010b. The variational approach to damage: II. The gradient damage models. *Comptes Rendus Mécanique* 338, 199–206. doi:[10.1016/j.crme.2010.03.012](https://doi.org/10.1016/j.crme.2010.03.012).
- Pham, K., Marigo, J.J., 2013. From the onset of damage to rupture: Construction of responses with damage localization for a general class of gradient damage models. *Continuum Mechanics and Thermodynamics* 25, 147–171. doi:[10.1007/s00161-011-0228-3](https://doi.org/10.1007/s00161-011-0228-3).
- Pham, K., Marigo, J.J., Maurini, C., 2011. The issues of the uniqueness and the stability of the homogeneous response in uniaxial tests with gradient damage models. *Journal of the Mechanics and Physics of Solids* 59, 1163–1190. doi:[10.1016/j.jmps.2011.03.010](https://doi.org/10.1016/j.jmps.2011.03.010).

- Rektorys, K., 1982. The method of discretization in time and partial differential equations. volume 4 of *Mathematics and its applications. East European series*. D. Reidel Publishing Company, Dordrecht, Holland.
- Rokoš, O., Zeman, J., Jirásek, M., 2015. Localization analysis of an energy-based fourth-order gradient plasticity model. URL: <http://arxiv.org/abs/1501.06788>, [arXiv:1501.06788](https://arxiv.org/abs/1501.06788).
- Roubíček, T., 2015. Maximally-dissipative local solutions to rate-independent systems and application to damage and delamination problems. *Nonlinear Analysis: Theory, Methods & Applications* 113, 33–50. doi:[10.1016/j.na.2014.09.020](https://doi.org/10.1016/j.na.2014.09.020).
- Simone, A., Askes, H., Sluys, L.J., 2004. Incorrect initiation and propagation of failure in non-local and gradient-enhanced media. *International Journal of Solids and Structures* 41, 351–363. doi:[10.1016/j.ijsolstr.2003.09.020](https://doi.org/10.1016/j.ijsolstr.2003.09.020).
- Thomas, M., Mielke, A., 2010. Damage of nonlinearly elastic materials at small strain – Existence and regularity results. *Zeitschrift für Angewandte Mathematik und Mechanik* 90, 88–112. doi:[10.1002/zamm.200900243](https://doi.org/10.1002/zamm.200900243).
- Vodička, R., Mantič, V., Roubíček, T., 2014. Energetic versus maximally-dissipative local solutions of a quasi-static rate-independent mixed-mode delamination model. *Meccanica* 49, 2933–2963. doi:[10.1007/s11012-014-0045-4](https://doi.org/10.1007/s11012-014-0045-4).

Appendix A. Numerical simulation of damage evolution

Evolution of the localized damage profile can be investigated numerically by solving a non-linear second-order differential equation that is valid within the damage zone, with appropriate continuity conditions imposed at the boundary of this zone. A particular feature of this problem is that the damage zone evolves and the position of its boundary is not known in advance. Numerical treatment of such a problem can be based on a modification of the shooting method.

Let us present the numerical procedure for the regularized elastic-brittle model constructed in Section 2 and analyzed in Section 3. For this model, the governing differential equation (31) reads

$$\ell_0^2 \omega_k''(x) + \frac{\mu_k}{(1 - \omega_k(x))^2} = 1 \quad (\text{A.1})$$

with $\mu_k = \sigma_k^2 / 2Eg_{f0}$ denoting a parameter that equals 1 at the onset of damage and then decreases to 0 during the failure process. At the onset of damage, we have $\omega_1(x) = 0$ and $\mu_1 = 1$. Eq. (A.1) should be solved successively for $k = 2, 3, \dots, N$ on intervals $\Omega_{d,k} = (-L_{d,k}/2, L_{d,k}/2)$ of unknown sizes $L_{d,k}$, taking into account boundary conditions (45) and (47).

Since the damage zone is centered at the origin and the solution is expected to be symmetric (given by an even function), we can impose symmetry condition (vanishing ω') at $x = 0$ and compute the values of damage for non-negative x only. The size of each step could be controlled by prescribing a certain (negative) increment of parameter μ . However, it is more convenient to specify the step size by prescribing the value of damage at $x = 0$, denoted as ω_{\max} , and consider the value of parameter μ as unknown. Thus, in a typical step number k , we have to find the values of μ_k and $L_{d,k}$ such that the solution $\omega_k(x)$ of Eq. (A.1) satisfies conditions

$$\omega_k(0) = \omega_{\max,k} \quad (\text{A.2})$$

$$\omega'_k(0) = 0 \quad (\text{A.3})$$

$$\omega_k(L_{d,k}/2) = \omega_{k-1}(L_{d,k}/2) \quad (\text{A.4})$$

$$\omega'_k(L_{d,k}/2) = \omega'_{k-1}(L_{d,k}/2) \quad (\text{A.5})$$

From the numerical point of view, conditions (A.2)–(A.3) can be considered as initial conditions, which would be sufficient to solve the problem if μ_k were known. For a selected trial value of μ_k , we can construct an approximate solution by a finite difference scheme and find the size of the damage zone $L_{d,k}$ from (A.5). If the yet unexploited condition (A.4) happens to be satisfied, the trial value of μ_k is correct and the solution is accepted. In general, it is necessary to adjust the trial value and iterate on it until (A.4) is satisfied with a prescribed tolerance.

To formalize the procedure described above, let us introduce a function $\tilde{\omega}(x, \mu)$ defined as the solution of Eq. (A.1) with μ_k set to μ and with initial conditions (A.2)–(A.3):

$$\ell_0^2 \frac{\partial^2 \tilde{\omega}(x, \mu)}{\partial x^2} + \frac{\mu}{(1 - \tilde{\omega}(x, \mu))^2} = 1 \quad (\text{A.6})$$

$$\tilde{\omega}(0, \mu) = \omega_{\max,k} \quad (\text{A.7})$$

$$\frac{\partial \tilde{\omega}(0, \mu)}{\partial x} = 0 \quad (\text{A.8})$$

Furthermore, let $\tilde{L}(\mu)$ be a function defined implicitly as the solution of

$$\frac{\partial \tilde{\omega}(\tilde{L}(\mu), \mu)}{\partial x} = \omega'_{k-1}(\tilde{L}(\mu)) \quad (\text{A.9})$$

and let $F(\mu)$ be a function defined as

$$F(\mu) = \tilde{\omega}(\tilde{L}(\mu), \mu) - \omega_{k-1}(\tilde{L}(\mu)) \quad (\text{A.10})$$

The objective is to find μ_k such that

$$F(\mu_k) = 0 \quad (\text{A.11})$$

This can be done iteratively by the Newton method, provided that we are able to evaluate the derivative $dF/d\mu$. Differentiation of (A.10) leads to

$$\frac{dF(\mu)}{d\mu} = \frac{\partial\tilde{\omega}(\tilde{L}(\mu), \mu)}{\partial x} \frac{d\tilde{L}(\mu)}{d\mu} + \frac{\partial\tilde{\omega}(\tilde{L}(\mu), \mu)}{\partial\mu} - \frac{d\omega_{k-1}(\tilde{L}(\mu))}{dx} \frac{d\tilde{L}(\mu)}{d\mu} \quad (\text{A.12})$$

By virtue of (A.9), the first term on the right-hand side cancels with the third term, and the formula simplifies to

$$\frac{dF(\mu)}{d\mu} = \frac{\partial\tilde{\omega}(\tilde{L}(\mu), \mu)}{\partial\mu} \quad (\text{A.13})$$

The partial derivative of $\tilde{\omega}$ with respect to μ can be obtained by linearization of (A.6)–(cond92) around the solution $\tilde{\omega}(x, \mu)$. Differentiation of both sides of (A.6) with respect to μ yields

$$\ell_0^2 \frac{\partial^3 \tilde{\omega}(x, \mu)}{\partial x^2 \partial \mu} + \frac{1}{(1 - \tilde{\omega}(x, \mu))^2} + \frac{2\mu}{(1 - \tilde{\omega}(x, \mu))^3} \frac{\partial \tilde{\omega}(x, \mu)}{\partial \mu} = 0 \quad (\text{A.14})$$

The derivative $\partial\tilde{\omega}/\partial\mu$, for convenience denoted as $\tilde{\omega}_\mu$, can thus be computed from the linear differential equation

$$\ell_0^2 \frac{\partial^2 \tilde{\omega}_\mu(x, \mu)}{\partial x^2} + \frac{2\mu}{(1 - \tilde{\omega}(x, \mu))^3} \tilde{\omega}_\mu(x, \mu) = -\frac{1}{(1 - \tilde{\omega}(x, \mu))^2} \quad (\text{A.15})$$

Since the right-hand sides of (A.7)–(A.8) do not depend on μ , the initial conditions for $\tilde{\omega}_\mu$ are

$$\tilde{\omega}_\mu(0, \mu) = 0 \quad (\text{A.16})$$

$$\frac{\partial \tilde{\omega}_\mu(0, \mu)}{\partial x} = 0 \quad (\text{A.17})$$

The complete algorithm can be summarized as follows:

1. Set $k = 1$, $\mu_1 = 1$, $\omega_1(x) = 0$, $\omega_{\max,1} = 0$.
2. Increment the step counter k and set $\omega_{\max,k} = \omega_{\max,k-1} + \Delta\omega_{\max}$.
3. Set $j = 0$ and find an initial guess $\mu_k^{(0)}$.
4. By the finite difference method on a grid consisting of points $x_i = i \Delta x$, $i = 0, 1, 2, \dots, n$, compute an approximate numerical solution $\tilde{\omega}_i$ of (A.6)–(A.8) with μ set to $\mu_k^{(j)}$, and simultaneously compute an approximate numerical solution $\tilde{\omega}_{\mu,i}$ of (A.15)–(A.17). Terminate the incrementation of i when $\tilde{\omega}_i - \tilde{\omega}_{i-1} \leq \omega_{k-1}(x_i) - \omega_{k-1}(x_{i-1})$, and denote the value of counter i for which this happens as i^* .

5. Set $F = \tilde{\omega}_{i^*} - \omega_{k-1}(x_{i^*})$ and $F' = \tilde{\omega}_{\mu, i^*}$.
6. Increment the iteration counter j and evaluate the updated approximation of parameter $\mu_k^{(j)} = \mu_k^{(j-1)} - F/F'$.
7. If $|F| > \epsilon$ (where ϵ is a prescribed tolerance), go to step 4.
8. Accept the converged solution and define the values

$$\omega_k(x_i) = \begin{cases} \tilde{\omega}_i & \text{for } 0 \leq i \leq i^* \\ \omega_{k-1}(x_i) & \text{for } i^* < i \leq n \end{cases} \quad (\text{A.18})$$

9. Print the loading parameter $\mu_k^{(j)}$, damage zone size $L_{d,k} = 2x^{i^*}$ and damage values $\omega_k(x_i)$. Compute and print other relevant quantities, such as the stress, strains, inelastic elongation and total elongation.
10. If $\omega_{\max, k} < 1$, go to step 2.

The numerical parameters that need to be specified are the tolerance, ϵ , the increment of maximum damage, $\Delta\omega_{\max}$, the spatial step, Δx , and the number of spatial steps, n , which should be large enough to make sure that $2n \Delta x$ is larger than the maximum possible size of the damage zone. Of course, $\Delta\omega_{\max}$ and Δx could be changed adaptively. It is also necessary to select a finite difference scheme for the discretization in space, which is applied in step 4.

For instance, if the central difference scheme is used, Eq. (A.6) is replaced by

$$\frac{\ell_0^2}{(\Delta x)^2} (\tilde{\omega}_{i+1} - 2\tilde{\omega}_i + \tilde{\omega}_{i-1}) + \frac{\mu}{(1 - \tilde{\omega}_i)^2} = 1 \quad (\text{A.19})$$

from which

$$\tilde{\omega}_{i+1} = 2\tilde{\omega}_i - \tilde{\omega}_{i-1} + \frac{(\Delta x)^2}{\ell_0^2} \left(1 - \frac{\mu}{(1 - \tilde{\omega}_i)^2} \right) \quad (\text{A.20})$$

This recursive evaluation is applied for $i = 1, 2, \dots, i^*$. The values at the first two grid points,

$$\tilde{\omega}_0 = \omega_{\max, k} \quad (\text{A.21})$$

$$\tilde{\omega}_1 = \tilde{\omega}_0 + \frac{(\Delta x)^2}{2\ell_0^2} \left(1 - \frac{\mu}{(1 - \tilde{\omega}_0)^2} \right) \quad (\text{A.22})$$

are determined from the initial conditions (A.7)–(A.8) combined with (A.19) written for $i = 0$. In a similar fashion, the discretized form of (A.15)–(A.17) leads to

$$\tilde{\omega}_{\mu, 0} = 0 \quad (\text{A.23})$$

$$\tilde{\omega}_{\mu, 1} = -\frac{(\Delta x)^2}{2\ell_0^2} \frac{1}{(1 - \tilde{\omega}_0)^2} \quad (\text{A.24})$$

$$\tilde{\omega}_{\mu, i+1} = 2\tilde{\omega}_{\mu, i} - \tilde{\omega}_{\mu, i-1} - \frac{(\Delta x)^2}{\ell_0^2} \left(\frac{1}{(1 - \tilde{\omega}_i)^2} + \frac{2\mu\tilde{\omega}_{\mu, i}}{(1 - \tilde{\omega}_i)^3} \right), \quad i = 1, 2, \dots, i^* \quad (\text{A.25})$$

In step 3 of the algorithm, an initial guess of the load parameter $\mu_k^{(0)}$ has to be specified. In the first step (i.g., for $k = 2$), the initial guess $\mu_2^{(0)} = 1 - \omega_{\max,2}$ can be obtained from the analytical expression (44) for the initial damage rate. In the subsequent steps, the initial guess can be computed by extrapolation of the dependence between ω_{\max} and μ based on their values from the previous steps.

For simplicity, the numerical approach has been presented for Eq. (31), which corresponds to the regularized elastic-brittle model with constant characteristic length. Its extension to Eq. (97), which corresponds to the most general regularized softening model with variable characteristic length and covers equations (76), (106) or (100) as special cases, is straightforward.